Technology

Molecular Cell

The Dynamics of mRNA Turnover Revealed by Single-Molecule Imaging in Single Cells

Graphical Abstract

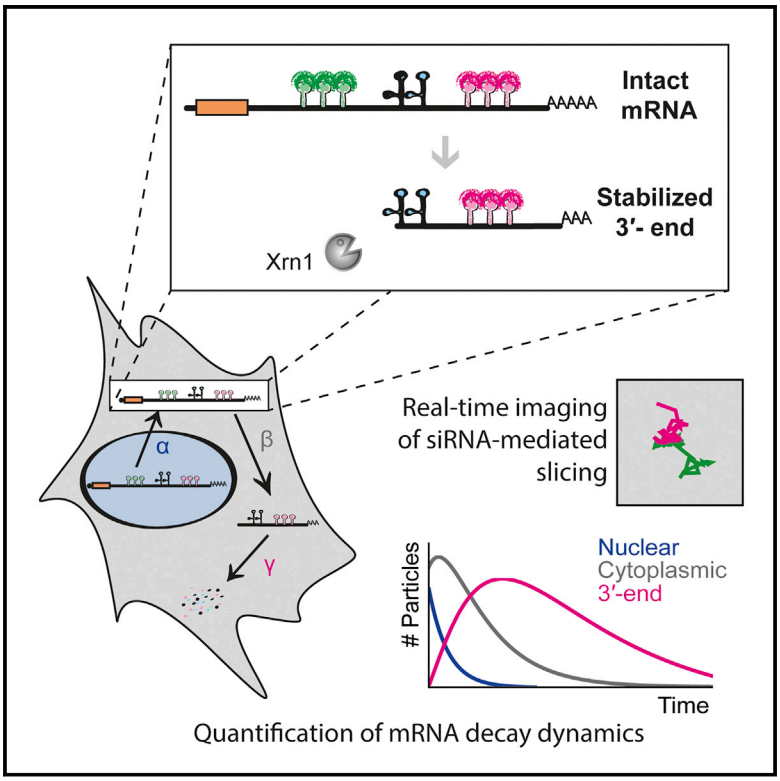

Authors

Ivana Horvathova, Franka Voigt, Anna V. Kotrys, ..., Michael B. Stadler, Luca Giorgetti, Jeffrey A. Chao

Correspondence

jeffrey.chao@fmi.ch

In Brief

RNA degradation plays a fundamental role in regulating gene expression. Horvathova et al. developed a fluorescence microscopy methodology that enables the dynamics of RNA degradation to be quantified with single-molecule resolution in fixed and living cells. This allows the entire life of mRNAs from birth to death to be visualized.

Highlights

- TREAT enables single-mRNA imaging of RNA degradation in single cells
- TREAT mRNA degradation does not burst
- Real-time observation of Ago2 slicing of TREAT mRNAs
- TREAT mRNAs are not degraded in P-bodies

Horvathova et al., 2017, Molecular Cell *68*, 1–11
November 2, 2017
https://doi.org/10.1016/j.molcel.2017.09.030

CellPress

Please cite this article in press as: Horvathova et al., The Dynamics of mRNA Turnover Revealed by Single-Molecule Imaging in Single Cells, Molecular Cell (2017), https://doi.org/10.1016/j.molcel.2017.09.030

Molecular Cell
Technology

CellPress

The Dynamics of mRNA Turnover Revealed by Single-Molecule Imaging in Single Cells

Ivana Horvathova,[1,2,4] Franka Voigt,[1,4] Anna V. Kotrys,[1] Yinxiu Zhan,[1,2] Caroline G. Artus-Revel,[1] Jan Eglinger,[1] Michael B. Stadler,[1,3] Luca Giorgetti,[1] and Jeffrey A. Chao[1,5,*]
[1]Friedrich Miescher Institute for Biomedical Research, 4058 Basel, Switzerland
[2]University of Basel, 4003 Basel, Switzerland
[3]Swiss Institute of Bioinformatics, 4058 Basel, Switzerland
[4]These authors contributed equally
[5]Lead Contact
*Correspondence: jeffrey.chao@fmi.ch
https://doi.org/10.1016/j.molcel.2017.09.030

SUMMARY

RNA degradation plays a fundamental role in regulating gene expression. In order to characterize the spatiotemporal dynamics of RNA turnover in single cells, we developed a fluorescent biosensor based on dual-color, single-molecule RNA imaging that allows intact transcripts to be distinguished from stabilized degradation intermediates. Using this method, we measured mRNA decay in single cells and found that individual degradation events occur independently within the cytosol and are not enriched within processing bodies. We show that slicing of an mRNA targeted for endonucleolytic cleavage by the RNA-induced silencing complex can be observed in real time in living cells. This methodology provides a framework for investigating the entire life history of individual mRNAs from birth to death in single cells.

INTRODUCTION

Gene expression is regulated by the abundance of mRNA. The levels of all cellular transcripts are determined by the balance between the rates of transcription in the nucleus and degradation in the cytoplasm. The life of an mRNA begins when it emerges from RNA Pol II and is recognized by factors that are responsible for its capping, splicing, and polyadenylation. The mature transcript is then exported to the cytoplasm where it can be transported, translated, and eventually degraded. While the importance of transcription in controlling gene expression is well established, it has become increasingly clear that the regulation of mRNA stability, particularly during development or rapid changes in environmental conditions, can dramatically influence mRNA levels (Elkon et al., 2010; Friedel et al., 2009; Hao and Baltimore, 2009; Miller et al., 2011; Rabani et al., 2011). RNA degradation also plays a crucial role in mRNA quality control that safeguards cells from the deleterious effects of aberrant transcripts (Isken and Maquat, 2007).

Degradation of mRNAs is a multi-step process that requires an orchestrated series of enzymatic reactions (Garneau et al., 2007). For most mRNAs, shortening of the poly(A) tail is thought to be the first step in mRNA decay and requires the consecutive actions of the Pan2-Pan3 and the Ccr4-Caf1-Tob complexes (Funakoshi et al., 2007; Yamashita et al., 2005). Following deadenylation, the 5′-cap structure is hydrolyzed by the Dcp1-Dcp2 complex (Dunckley and Parker, 1999; Lykke-Andersen, 2002; van Dijk et al., 2002). The body of the transcript can then be degraded by Xrn1 (5′-to-3′ exonuclease) or the cytoplasmic exosome complex (3′-to-5′ exonuclease) (Garneau et al., 2007). Currently, Xrn1-mediated degradation is believed to be the dominant cytoplasmic decay pathway, perhaps through the coupling of Xrn1 to Dcp1-Dcp2 by the scaffold protein Edc4 (Chang et al., 2014). Additional mRNA decay pathways have also been identified that enable regulation of mRNA stability (e.g., AU-rich elements, miRNAs) or quality control (Garneau et al., 2007; Schoenberg and Maquat, 2012).

While many of the proteins and pathways involved in mRNA degradation have been elucidated, our understanding of when and where these events occur within cells has not kept pace. Single-molecule fluorescent *in situ* hybridization (smFISH) has enabled some aspects of mRNA degradation to be characterized, but the loss of signal resulting directly from the process being studied has prevented this approach from being widely applied (Kramer, 2017; Trcek et al., 2011, 2013). Here, we describe a single-molecule fluorescent microscopy methodology for measuring the spatial and temporal dynamics of mRNA degradation in fixed and living single cells.

DESIGN

Recently, a viral RNA pseudo-knot (PK) structure was identified in flaviviruses that blocks Xrn1 by sequestering the 5′-phosphate from the enzyme, thereby preventing further degradation of the viral genome (Kieft et al., 2015). We took advantage of this feature to engineer a single-molecule mRNA turnover biosensor that contains a 3′ UTR with the tandem PKs from the Kunjin strain of West Nile virus placed between the orthogonal PP7 and MS2 bacteriophage stem loops (Chapman et al., 2014a; Hocine et al., 2013) (Figure 1A). Since the MS2 stem loops are protected from

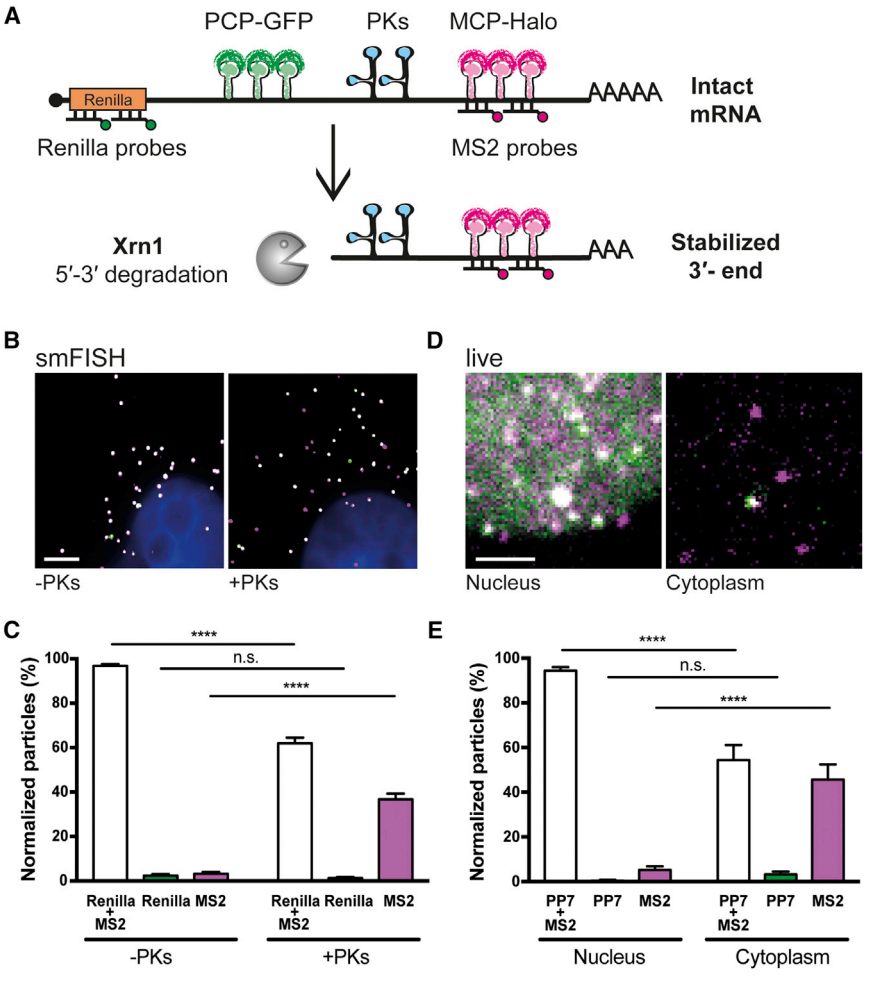

Figure 1. TREAT Imaging of mRNA Degradation in Single Cells

(A) Schematic of the intact TREAT reporter mRNA and its stabilized degradation fragment. *Renilla* luciferase is in the open reading frame, and the 3′ UTR contains two viral pseudo-knots (PKs, blue) that are flanked by PP7 (green) and MS2 (magenta) stem loops. The stabilized 3′ end (MS2 stem loops only) arises from partial degradation by Xrn1 that is blocked by the PKs. In fixed cells, smFISH probes can be targeted to *Renilla* luciferase and MS2 stem loops, and in live cells, PP7 and MS2 coat proteins (PCP and MCP, respectively) can be fused to spectrally distinct fluorescent proteins.

(B) Representative smFISH images of HeLa cells stably expressing control (−PKs) or TREAT (+PKs) reporters hybridized with *Renilla* (green) and MS2 (magenta) probes. Cells were induced by addition of doxycycline for 2 hr and fixed 2 hr after induction was stopped. Scale bar, 2 μm.

(C) Viral PKs are required for accumulation of stabilized 3′ ends. Quantitative analysis of smFISH reveals that the fraction of intact transcripts (*Renilla* + MS2, white) decreases while the fraction of stabilized 3′ ends (MS2, magenta) increases in cells expressing TREAT reporter (10,810 particles, 62 cells) compared to control reporter (3,465 particles, 66 cells) (p values, **** < 0.0001; n.s., not significant; unpaired t test). Graph shows mean ± SEM.

(D) Representative live-cell images of a HeLa cell line stably expressing the TREAT reporter with NLS-PCP-GFP and NLS-MCP-Halo. Intact mRNAs are dual labeled with NLS-MCP-Halo (magenta) and NLS-PCP-GFP (green) and appear as white spots, whereas stabilized 3′ ends are labeled by only NLS-MCP-Halo.

(E) TREAT mRNAs are degraded in the cytoplasm. Quantification of intact and degraded RNAs in the nucleus (388 particles, 11 cells) and cytoplasm (594 particles, 12 cells) was performed using two-color SPT, and co-localization analysis was normalized by detection efficiencies in both channels. p values, **** < 0.0001; n.s., not significant; unpaired t test.

Xrn1-mediated degradation by the PKs, this biosensor allows discrimination between intact (PP7 and MS2) transcripts and stabilized 3′ end degradation intermediates (MS2 only) in living cells that express the PP7 coat protein (PCP) and MS2 coat protein (MCP) fused to spectrally distinct fluorescent proteins. Similarly, smFISH probes can be targeted to the two distinct regions of the transcript in order to image mRNA decay in fixed cells. We refer to this technique as 3(*three*)′-*R*NA *e*nd *a*ccumulation during *t*urnover (TREAT).

RESULTS

Development of TREAT for Imaging mRNA Degradation

In order to monitor physiological mRNA decay, expression of the TREAT reporter should not disrupt Xrn1-mediated degradation. While Xrn1 does not form a stable complex with the viral PKs, it has been reported that overexpression of the entire Kunjin flaviviral subgenomic RNA, which contains the PKs and other structured RNA elements, results in stabilization of endogenous mRNAs (Chapman et al., 2014b; Moon et al., 2012). The stability of endogenous c-Myc mRNA measured by RT-qPCR was similar in HeLa cells that expressed the TREAT reporter and cells that did not express it (Figure S1A). Importantly, the PKs also did not alter the stability or translation of the TREAT reporter compared to a control lacking these elements (Figures S1B and S1C). To validate the potential of the PKs to block Xrn1 from fully degrading the TREAT reporter, we determined the size of TREAT and control transcripts by northern blot. A probe complementary to a sequence in the 3′ UTR in both types of transcripts demonstrated that accumulation of the specific degradation intermediate occurred only in the presence of the PKs (Figure S2). Importantly, co-expression of NLS-MCP-Halo and NLS-PCP-GFP did not stabilize alternative degradation intermediates of the reporters without PKs as reported in yeast (Figure S2) (Garcia and Parker, 2015; Heinrich et al., 2017). Taken as a whole, the presence of the viral PKs in the TREAT reporter does not perturb RNA degradation in either *cis* or *trans* in HeLa cells.

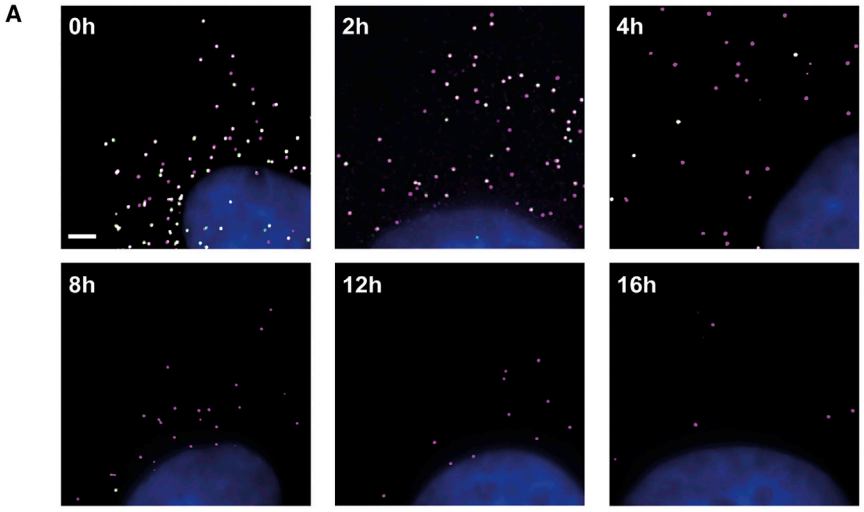

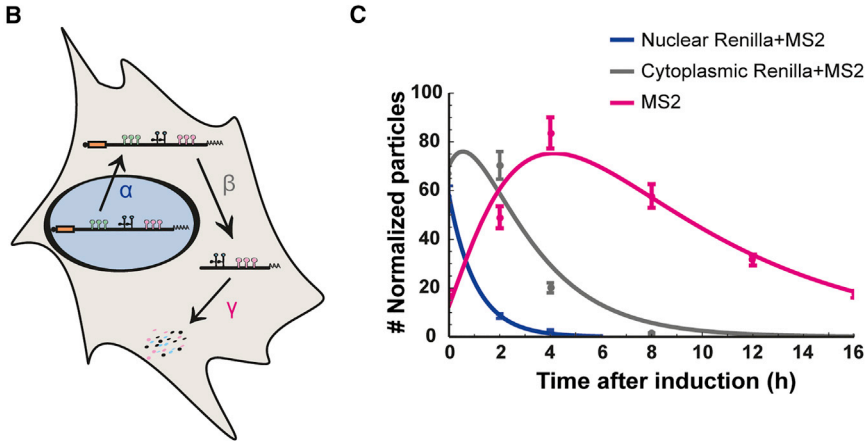

Figure 2. Half-Life Measurement of TREAT mRNAs in Single Cells

(A) Representative smFISH images of the TREAT reporter in HeLa cells. Cells were induced for 2 hr with doxycycline and fixed at successive time points (0, 2, 4, 8, 12, 16 hr) after induction was stopped. Images show that the stabilized 3′ end (MS2, magenta) accumulates within cells while the number of intact TREAT mRNAs (*Renilla* + MS2, white) decreases over time. Scale bar, 2 μm.

(B) Schematic model of the TREAT mRNA life cycle within a cell with depicted rates: α, nuclear export rate; β, degradation rate of the TREAT transcript; γ, stabilized 3′ end degradation rate.

(C) Counts of intact mRNAs (nuclear or cytoplasmic) and stabilized 3′ ends were obtained from the quantitative analysis of smFISH data at fixation time points (> 120 cells per time point in two biological replicates). Data were fit to the model to calculate the experimental rate constants (α, β, γ). All error bars indicate SEM.

The TREAT reporter was integrated into a single genomic locus in doxycycline-inducible HeLa cells that stably express NLS-PCP-GFP and NLS-MCP-Halo to monitor mRNA turnover in single cells. The ability of TREAT to detect mRNA degradation requires quantification of the co-localization of fluorescent signals positioned 5′ and 3′ of the PKs. To this aim, a control reporter without PKs was used to benchmark co-localization and determine detection efficiencies in both fixed and living cells, since only intact two-color transcripts should be detected with this construct (Figure S3, Movie S1). In fixed cells, smFISH probes targeting the *Renilla* luciferase coding sequence and MS2 stem loops demonstrated that introduction of the PKs into the TREAT reporter enabled detection of an increase in the fraction of MS2-only particles (Figures 1B and 1C). Importantly, there was no change in the number of *Renilla*-only particles, indicating the effect of the PKs was specific for the stabilized 3′ end. In live cells, single-particle tracking (SPT) of TREAT mRNAs in the nucleus demonstrated that the majority of transcripts are intact (> 94%) (Figures 1D and 1E, Movie S2). In the cytoplasm, however, SPT and co-localization analysis of TREAT transcripts revealed two distinct populations of RNA, intact mRNAs (MS2 and PP7) and stabilized 3′ ends (MS2 only) (Figures 1D and 1E). Similar to the fixed-cell data, there was no increase in the number of PP7-only-labeled particles. These experiments demonstrated that TREAT can measure mRNA turnover with single-molecule resolution in both fixed and living cells.

TREAT Measurement of mRNA Degradation in Single Cells

We measured the kinetics of TREAT mRNA degradation in single cells using smFISH. Expression of the reporter was induced for 2 hr with doxycycline, and cells were fixed at successive time points after induction was stopped (Figure 2A). The turnover of intact TREAT mRNAs and the stabilized 3′ ends in the cytoplasm can be described by

$$\frac{d[\mathrm{Nuc}]}{dt} = -\alpha[\mathrm{Nuc}]$$

$$\frac{d[\mathrm{Cyt}]}{dt} = \alpha[\mathrm{Nuc}] - \beta[\mathrm{Cyt}]$$

$$\frac{d[\mathrm{Deg}]}{dt} = \beta[\mathrm{Cyt}] - \gamma[\mathrm{Deg}],$$

where *Nuc* is the number of intact nuclear mRNAs, α is the export rate of mRNAs to the cytoplasm, *Cyt* is the number of intact cytoplasmic mRNAs, β is the decay rate of the intact cytoplasmic mRNA, *Deg* is the number of stabilized 3′ ends, and γ is the decay rate of the stabilized 3′ ends (Figure 2B). Fitting the evolution of the mean numbers of RNA species in time to this model resulted in an export time of 0.74 ± 0.05 hr and degradation half-lives of 1.63 ± 0.24 hr (cytoplasmic intact mRNA) and 4.39 ± 0.47 hr (stabilized 3′ end) (Figure 2C). RNAi knockdown

of Xrn1 increased the half-life of the TREAT reporter while knockdown of Rrp40, an exosome core subunit, had no effect, indicating that Xrn1-mediated degradation is indeed the dominant decay pathway for TREAT transcripts (Figure S4).

Single-cell measurements enabled the observation that transcription is not a simple Poisson process and can occur in bursts; however, it has not yet been possible to determine if similar dynamics also occur during mRNA turnover (Raj and van Oudenaarden, 2008). During analysis of the smFISH images, we observed considerable cell-to-cell variation in the abundance of stabilized 3′ ends in individual cells. The ratio of the variance to the mean (Fano factor) of the number of stabilized 3′ ends at each time point was greater than one, which is indicative of possible deviations from Poisson processes. To determine the nature of this variability, we used a discrete stochastic approach to solve the master equation associated with the model described above and generated the probability distribution of intact mRNAs and stabilized 3′ ends based upon their distribution at the initial time point. Simulation of the RNA populations at later time points, assuming that the turnover of intact and degraded mRNA are single-step Poisson processes governed by the measured decay rates, was in good agreement with the experimental data (Figure S5). Virtually all of the variability in the number of stabilized 3′ ends of the TREAT transcript could be accounted for by the initial cell-to-cell heterogeneity in mRNA numbers that results from variable levels of transcription in individual cells. This indicates that the degradation of each TREAT transcript occurs independently within the cell.

Real-Time Observation of mRNA Degradation in Living Cells

Due to the difference in timescales between the half-life of the TREAT mRNA (1.6 hr) and our live-cell experiments (5–10 s), it was challenging to directly detect TREAT degradation events in live cells. In order to generate a TREAT reporter that would be more rapidly degraded, we incorporated an siRNA sequence derived from Firefly luciferase between the PP7 stem loops and the PKs and stably expressed the corresponding shRNA in the HeLa cell line used for imaging (Figure 3A). Using smFISH, the cytoplasmic half-life of the TREAT siRNA reporter was determined to be ~7.5 min, while the export time and degradation of the stabilized 3′ ends were not changed (Figure 3B). We were also able to detect the transient appearance of the 5′ end of the transcript in the cytoplasm generated by Ago2-mediated endonucleolytic cleavage, which was degraded with a half-life of ~9.7 min. Similar to our modeling of the variability of TREAT reporter degradation, we also did not detect degradation bursts for TREAT siRNA transcripts (Figure S6).

In order to identify the cellular site of slicing, we imaged the TREAT siRNA reporter in live cells. While RNAi factors have been detected in the nuclei of mammalian cells, they were found to be inactive and unable to degrade nuclear transcripts (Zeng and Cullen, 2002). Recently, however, it has been suggested that Ago2 can be active in mammalian cell nuclei and was shown to degrade the nuclear lncRNA Malat1 (Gagnon et al., 2014). We quantified the co-localization of nuclear TREAT siRNA transcripts and did not observe a change in the number of intact transcripts, 5′ ends, or stabilized 3′ ends compared to a non-sliced control, indicating that the short half-life of TREAT siRNA transcripts was not due to increased nuclear degradation (Figures 3C and 3D).

To quantify cytoplasmic slicing, we developed an automated SPT and co-localization algorithm to identify degradation events within our movies. We reasoned that slicing could be visualized as either the rapid disappearance of the 5′ signal (NLS-PCP-GFP) from a dual-labeled transcript or the spatial separation of the 5′ signal (NLS-PCP-GFP) and 3′ signal (NLS-MCP-Halo) after endonucleolytic cleavage (Figure 4A). Loss of the 5′ signal (NLS-PCP-GFP) from a transcript could arise from either slicing or photo-bleaching. We measured the slope of the loss of NLS-PCP-GFP and did not detect any significant outliers for intact TREAT siRNA transcripts compared to a non-sliced control (Figure 4B). We did, however, detect slicing decay events (n = 17) where intact mRNAs were observed to sever into 5′ ends (PP7) and 3′ ends (MS2) that then spatially move apart from one another and could be independently tracked (Figure 4C, Movie S3). Since the 5′ end is not immediately degraded and can separate from its 3′ end after Ago2-mediated endonucleolytic cleavage, this suggests that there is not a tight coupling between slicing and the downstream degradation of the decay intermediates. We measured the cytoplasmic position of slicing events from the nucleus and found that their distribution was similar to non-sliced control transcripts, indicating that slicing does not preferentially occur in a specific location, but is homogenously distributed throughout the cell (Figure 4D).

P-Bodies Are Not Sites of TREAT mRNA Degradation

Phase transitions have been implicated in an increasing number of diverse biological phenomena; however, their underlying molecular mechanisms are not well understood (Banani et al., 2017). Processing bodies (P-bodies), evolutionarily conserved membrane-less cytoplasmic compartments that are formed by the condensation of RNA-binding proteins and mRNAs, were one of the first phase transitions to be identified (Jain and Parker, 2013). Since they are enriched for proteins involved in many aspects of mRNA turnover, including decapping factors, deadenylases, and Xrn1, it was initially proposed that they functioned as cellular sites of active mRNA degradation (Cougot et al., 2004; Sheth and Parker, 2003). Subsequently, it was shown that microscopically visible P-bodies accounted for only a small fraction (~0.3%) of the cytoplasmic volume and were not required for degradation of transcripts, indicating that mRNA turnover does not require compartmentalization (Chu and Rana, 2006; Eulalio et al., 2007; Leung et al., 2006; Stoecklin et al., 2006). Whether mRNA decay, however, was more efficient or inhibited within P-bodies remained an open question. It has also been suggested that P-bodies function as sites of mRNA storage during cellular stress from which mRNAs return to the cytoplasm for translation upon recovery (Bhattacharyya et al., 2006; Brengues et al., 2005). Since the TREAT reporter can directly report on the cellular site of mRNA decay, we set out to clarify the role of P-bodies in this process.

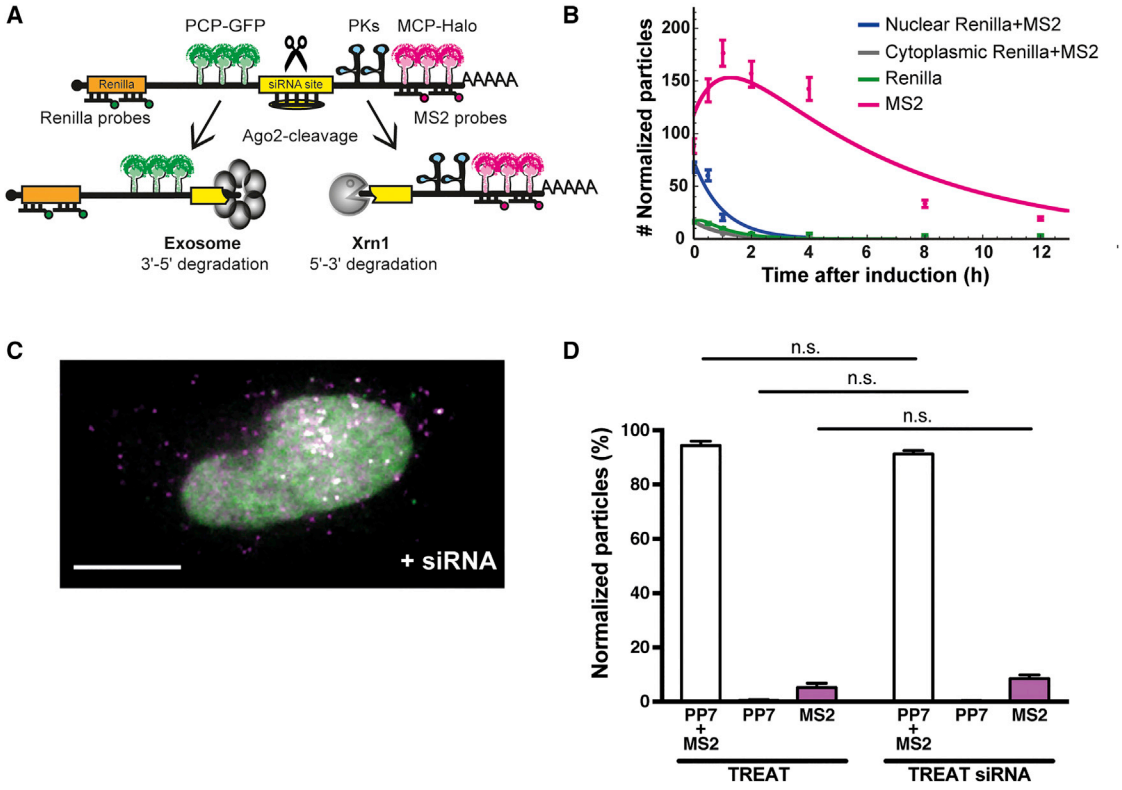

Figure 3. TREAT siRNA Transcripts Are Rapidly Degraded in the Cytoplasm

(A) Schematic of TREAT siRNA reporter and slicing degradation fragments. An siRNA target sequence was placed between the PP7 stem loops and the PKs in the 3′ UTR. After expression of the cognate siRNA, endonucleolytic cleavage results in a 5′ end containing PP7 stem loops and the stabilized 3′ end containing MS2 stem loops.

(B) Measurement of TREAT siRNA reporter stability. Counts of intact mRNA (nuclear or cytoplasmic), 5′ ends, and stabilized 3′ ends were obtained from quantification of smFISH data (> 190 cells per time point in two biological replicates).

(C) Representative live-cell image of HeLa cells expressing TREAT siRNA reporter labeled with NLS-PCP-GFP (green) and NLS-MCP-Halo (magenta). Intact mRNAs are dual labeled with NLS-PCP-GFP (green) and NLS-MCP-Halo (magenta) and appear as white spots. Scale bar, 10 μm.

(D) Quantification of co-localization of NLS-PCP-GFP and NLS-MCP-Halo for TREAT siRNA reporter in the nucleus (534 particles, 14 cells) compared to nuclear TREAT data (388 particles, 11 cells) (p values: n.s., not significant; unpaired t test).

A HeLa cell line was generated that stably expresses a SNAP-Dcp1a fluorescent fusion protein, which labels P-bodies, in combination with NLS-PCP-GFP and NLS-MCP-Halo, which allowed imaging of P-bodies and TREAT reporter mRNAs in living cells (Kedersha and Anderson, 2007). The number of SNAP-Dcp1a-labeled P-bodies detected by live-cell imaging was similar to the number of endogenous P-bodies detected by immunofluorescence against DDX6, an established P-body marker, and the foci formed by SNAP-Dcp1a also co-localized with endogenous Xrn1 (Figure S7). We then assessed the co-localization of intact and degraded TREAT transcripts with P-bodies in living cells. Simultaneous acquisition of the TREAT reporter in two channels (NLS-PCP-GFP, NLS-MCP-Halo) was followed by imaging of P-bodies (SNAP-Dcp1a). P-bodies were segmented and used to generate distance maps where positions within P-bodies were defined as positive values while locations outside received negative values. P-body co-localization of intact and degraded TREAT transcripts was measured at each time point. A cumulative P-body localization index was calculated from three consecutive frames (3 × 50 ms) in order to account for spurious co-localization. This index was negative for all intact TREAT transcripts and stabilized 3′ ends, indicating that neither species accumulated in P-bodies (Figures 5A and 5B, Movie S4).

Transcripts that contain an AU-rich element (ARE) within their 3′ UTRs undergo rapid degradation, and this *cis*-acting element has also been shown to promote the association of mRNAs with P-bodies (Franks and Lykke-Andersen, 2007). We modified the TREAT reporter to include the TNF-α ARE between the PP7 stem loops and the viral PKs (Figure 5C). The half-life of TREAT TNF-α ARE reporter transcripts was reduced to ~30 min, which is consistent with the role of the ARE on mRNA stability (Figure S8). Interestingly, we also found that the nuclear export rate and the degradation of the stabilized 3′ ends was faster for the TREAT TNF-α ARE reporter. We detected a small number of intact TREAT ARE transcripts with positive cumulative P-body localization values; however, we found no evidence for the accumulation of degraded fragments within P-bodies (Figures 5C and 5D, Movie S5). To confirm that the RNAs within P-bodies were not a mixture of

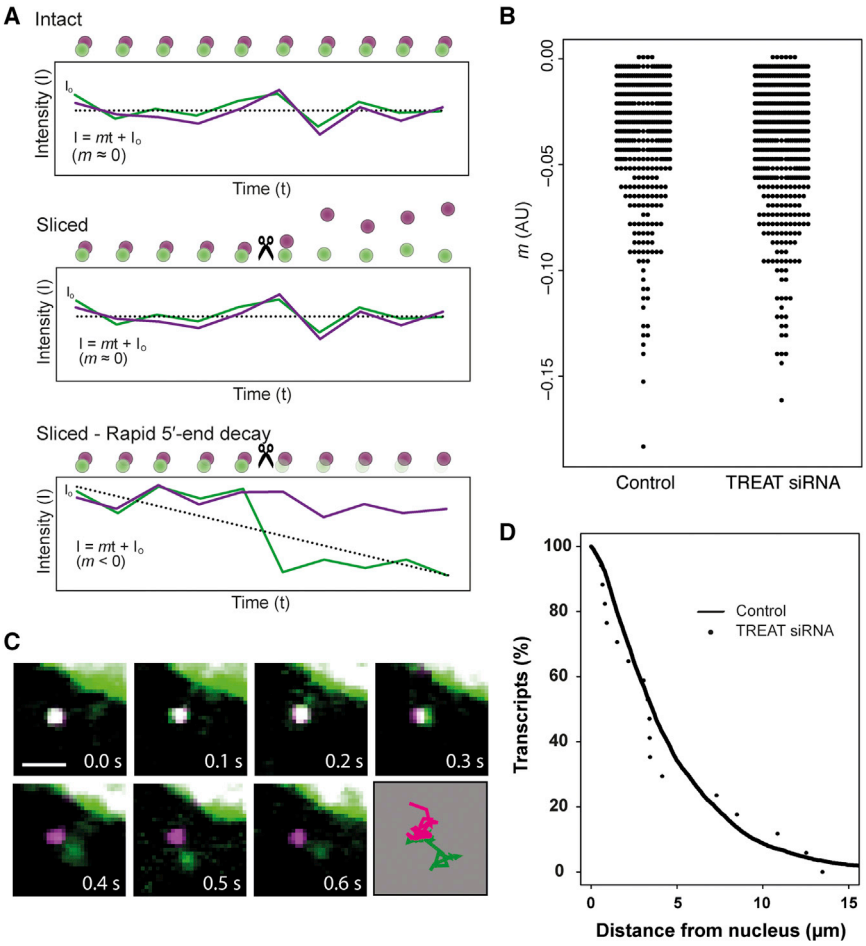

Figure 4. TREAT Imaging of siRNA-Mediated Endonucleolytic Cleavage in Live Cells

(A) Cartoons depicting potential slicing scenarios in live cells. Non-sliced: Dual-labeled transcripts have green and magenta signals that co-localize and do not change in fluorescence intensity (I) over time (t) compared to initial intensity (I_0). Dotted lines show theoretical linear fits to the bleach-corrected fluorescence intensity of the green signal curves. The slope (m) of the linear regression was used to quantify intensity changes. Sliced: Dual-labeled transcripts are cleaved between green and magenta signals that can independently be tracked. Sliced and rapid 5′ end decay: After slicing of a dual-labeled transcript, the green signal is rapidly lost.

(B) Beeswarm plot of the slopes (m) of the linear regressions of the bleach-corrected NLS-PCP-GFP intensities of dual-labeled particles (> 5 frames) collected for the TREAT siRNA reporter (575 particles, 681 cells) as well as the non-sliced control (361 particles, 125 cells). Populations do not differ in their outlier composition. In control data, 5% of m are less than −0.093, and an almost identical fraction of TREAT siRNA reporters (5.4%) are also within this threshold.

(C) Time sequence showing a slicing event in a live cell. A dual-colored intact mRNA (PP7 + MS2) is observed for several consecutive frames followed by slicing and spatial separation of the 5′ (PP7, green) and 3′ (MS2, magenta) fragments. Time series projection of two-channel SPT shows co-localization and separation of signals.

(D) Distribution of slicing events in the cytoplasm. The location of slicing events (black dots) relative to the nucleus is similar to the positions of control transcripts (black line). p value = 0.74; Kolmogorov-Smirnov test. All error bars indicate SEM. Scale bar, 1 μm.

intact mRNAs and stabilized 3′ ends resulting from active degradation, we compared the ratio of the fluorescence intensity of NLS-PCP-GFP to NLS-MCP-Halo for RNAs in P-bodies with intact transcripts that remained in the cytosol (Figure 5E). The RNAs in P-bodies and intact mRNAs in the cytosol had similar ratios, indicating that RNAs within P-bodies were intact and were not undergoing degradation.

Since the number of P-bodies is low in unstressed cells, we stressed cells with arsenite for 1 hr to increase the number and size of P-bodies. It has been proposed previously that cellular transcripts may be triaged through stress granules into P-bodies for degradation during stress (Anderson et al., 2015; Decker and Parker, 2012). During arsenite stress, we detected only intact TREAT mRNAs and not stabilized 3′ ends with positive cumulative P-body localization values (Figures 6A and 6B, Movie S6). To increase the association of mRNAs with P-bodies, we added a 5′-TOP sequence to the TREAT reporter, because this *cis*-element was shown to promote the interaction of mRNAs with P-bodies during arsenite stress (Halstead et al., 2015). Similarly, only intact 5′-TOP TREAT transcripts were found within P-bodies during stress (Figures 6C and 6D, Movie S7). Further experiments will be required to determine if P-bodies are sites of specialized mRNA degradation, but our data suggest that these cellular compartments are not general sites of active mRNA turnover during normal cell growth or stress.

Translation Inhibition Stabilizes TREAT mRNAs

While analyzing the spatial position of TREAT transcripts during stress, we observed an increase in the total number of intact mRNAs within cells (Figures 7A and 7B). Since only a small percentage of TREAT reporter transcripts accumulate in P-bodies or stress granules during arsenite stress, this increase in stability cannot be explained by these cellular compartments serving as protective storage sites. Because arsenite stress inhibits general translation via eIF2α phosphorylation, we tested the effect of several other translation inhibitors, which target distinct stages of protein synthesis, for their effects on mRNA stability. TREAT transcripts were induced for 2 hr with doxycycline followed by addition of harringtonine, cycloheximide, or puromycin (Figure 7C). Similar to arsenite, these translation inhibitors caused a dramatic stabilization of TREAT transcripts (Figure 7D). The effect was more pronounced after 4 hr of treatment with translation inhibitors, as

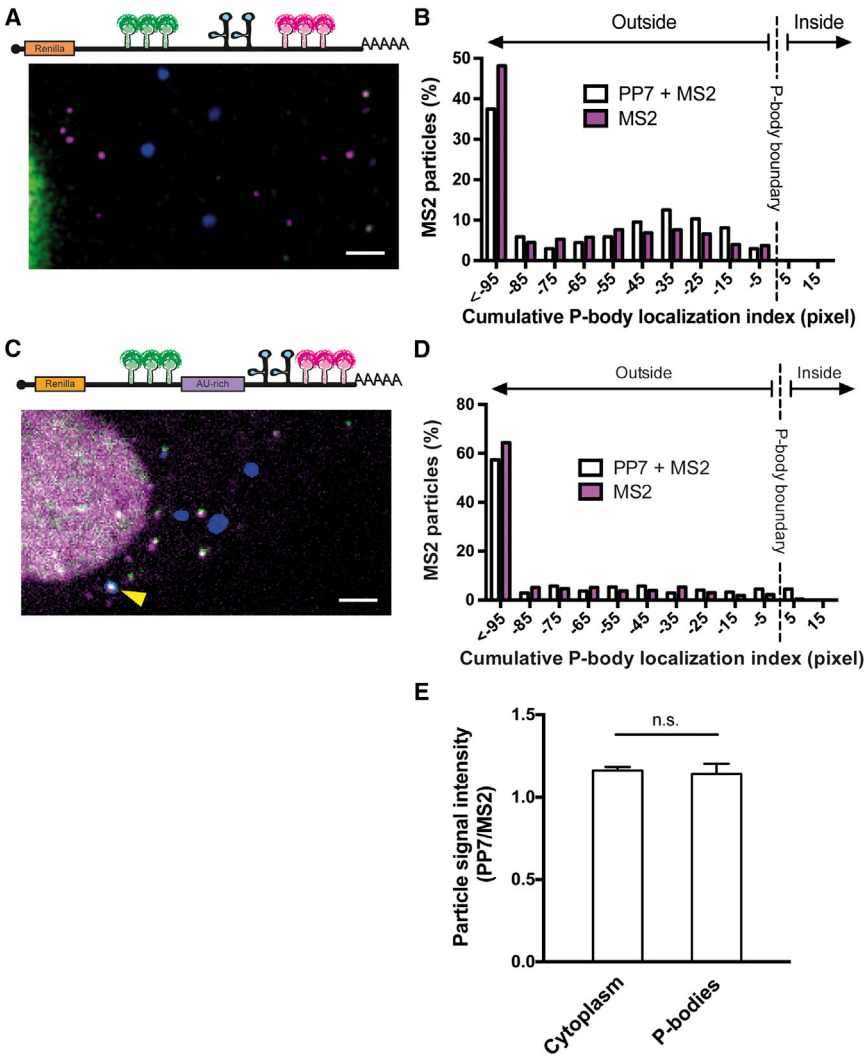

Figure 5. TREAT Transcripts Are Not Degraded in P-Bodies

(A) Representative live-cell image of TREAT reporter in HeLa cells expressing NLS-MCP-Halo (magenta), NLS-PCP-GFP (green), and SNAP-Dcp1a (blue).

(B) TREAT transcripts do not accumulate in P-bodies. Two-channel SPT identified intact (PP7 + MS2) and stabilized 3′ ends (MS2) (516 particles, 27 cells) in cells. The position in pixels of all RNAs with respect to P-bodies was measured, and the cumulative P-body localization index was calculated from three successive frames (3 × 50 ms).

(C) Representative live-cell image of TREAT TNF-α ARE reporter in HeLa cells expressing NLS-MCP-Halo (magenta), NLS-PCP-GFP (green), and SNAP-Dcp1a (blue). The yellow arrowhead points to an intact TREAT mRNA bound to a P-body.

(D) Low accumulation of intact TREAT TNF-α ARE transcripts within P-bodies. SPT identified intact (PP7 + MS2) and stabilized 3′ ends (MS2) (772 particles, 55 cells).

(E) Intact mRNAs in P-bodies are not undergoing degradation. The ratio of the fluorescent intensity of NLS-PCP-GFP and NLS-MCP-Halo was similar for all dual-colored mRNAs in P-bodies and cytosol (n.s., not significant; unpaired t test). Histograms are plotted with bin widths of 10 pixels. Scale bars, 5 μm. Error bars indicate SEM.

degradation remained completely blocked. While harringtonine and cycloheximide could immobilize ribosomes on TREAT transcripts, thereby blocking Xrn1 degradation, puromycin causes disassociation of ribosomes from transcripts. Our data indicate that any inhibition of translation results in stabilization of TREAT mRNAs.

The global inhibition of mRNA degradation we observed during arsenite stress is consistent with a general inhibition of decay resulting from proteolytic degradation of Tob and Pan3, which are the factors responsible for recruitment of deadenylases to transcripts (Yamagishi et al., 2014). Inhibition of deadenylation has also been observed in yeast and mammalian cells in response to a variety of cellular stresses, suggesting that this may be a conserved pathway that is activated when translation is inhibited (Gowrishankar et al., 2006; Hilgers et al., 2006). Alternatively, the release factor eRF3 has also been shown to compete with Tob/Pan3 for PABPC1, suggesting a possible direct coupling between translation and mRNA decay (Funakoshi et al., 2007; Yamagishi et al., 2014).

DISCUSSION

Single-molecule measurements of the mRNA life cycle have profoundly altered our understanding of gene expression; however, it has not yet been possible to directly measure how these processes are inter-connected within single cells. The continued development of multicolored RNA biosensors will enable a more sophisticated investigation of the coupling between transcription, translation, and mRNA degradation. A variety of orthogonal fluorescent proteins and RNA-labeling methods exist that would enable translation (TRICK) and mRNA turnover (TREAT) to be imaged simultaneously in three channels (Chen et al., 2009; Daigle and Ellenberg, 2007; Grimm et al., 2015; Halstead et al., 2015). Similarly, TREAT could also be coupled with the recently developed methods for nascent polypeptide imaging that would allow the relationship between translation and mRNA turnover to be understood in greater detail (Morisaki et al., 2016; Pichon et al., 2016; Wang et al., 2016; Wu et al., 2016; Yan et al., 2016). A complete accounting of an individual transcript's life from birth to death is now possible.

Limitations

Previously, overexpression or viral infection of RNAs containing Xrn1-blocking PKs was shown to affect degradation of endogenous mRNAs (Moon et al., 2012). While TREAT and a conceptually similar approach using Xrn1-resistant RNA elements did not

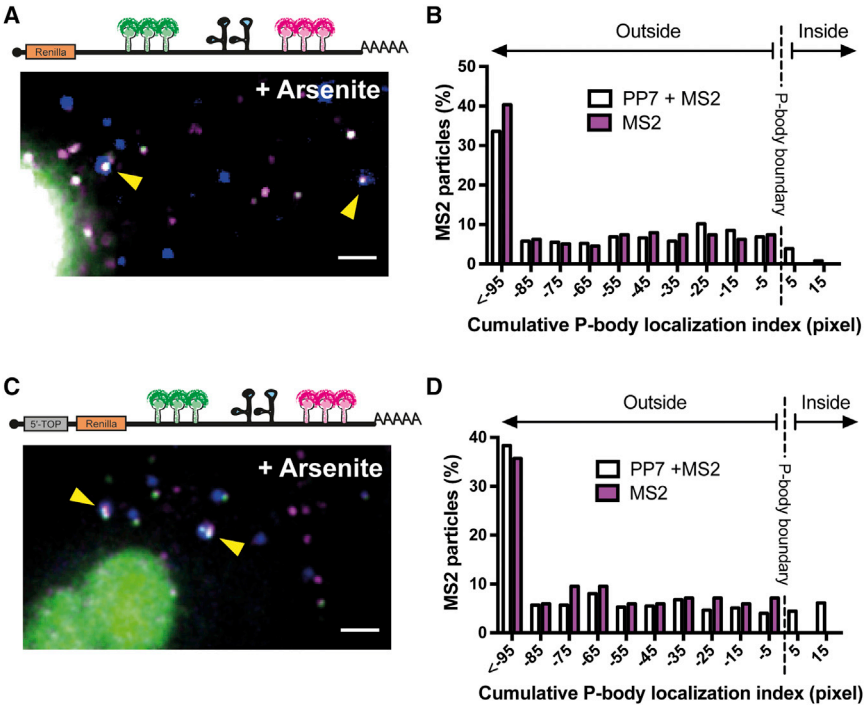

Figure 6. TREAT Transcripts Are Not Degraded in P-Bodies during Stress

(A) Representative live-cell image of TREAT reporter in HeLa cells expressing NLS-MCP-Halo (magenta), NLS-PCP-GFP (green), and SNAP-Dcp1a (blue) as a P-body marker stressed with arsenite (500 μM) for 1 hr.

(B) Intact TREAT transcripts accumulate in P-bodies during arsenite stress. SPT experiments were performed to identify intact (MS2 + PP7, white) and stabilized 3′ ends (MS2 only, magenta) in arsenite-stressed cells (539 particles, 19 cells).

(C) Representative live-cell image of 5′-TOP TREAT reporter in HeLa cells expressing NLS-MCP-Halo (magenta), NLS-PCP-GFP (green), and SNAP-Dcp1a (blue) as a P-body marker stressed with arsenite (500 μM) for 1 hr.

(D) Intact 5′-TOP TREAT transcripts accumulate in P-bodies during arsenite stress to a greater extent than TREAT transcripts. SPT experiments were performed to identify intact (MS2 + PP7, white) and stabilized 3′ ends (MS2 only, magenta) in arsenite-stressed (556 particles, 22 cells) cells. Histograms are plotted with bin widths of 10 pixels and centered at shown values. Scale bar, 5 μm.

detect inhibition of endogenous mRNA decay, this effect could be concentration dependent (Boehm et al., 2016). It will be an important control when establishing TREAT in other experimental systems that the approach itself does not influence mRNA degradation.

In order to directly detect mRNA decay events in live cells, we incorporated an siRNA target sequence within the TREAT reporter to shorten the half-life of the transcript. Continued development of automated SPT and analysis routines will enable the detection of decay events for more stable transcripts. Furthermore, tethering of TREAT reporter mRNAs to cytoplasmic structures (e.g., membranes via addition of a CAAX prenylation sequence to MCP) can immobilize the transcript and has been shown to allow monitoring of individual mRNAs for extended time periods (Yan et al., 2016). While restricting mobility of mRNAs may not be appropriate for all applications of TREAT, it will overcome limitations in decay detection due to movement of RNAs. Alternatively, advances in the speed and sensitivity of

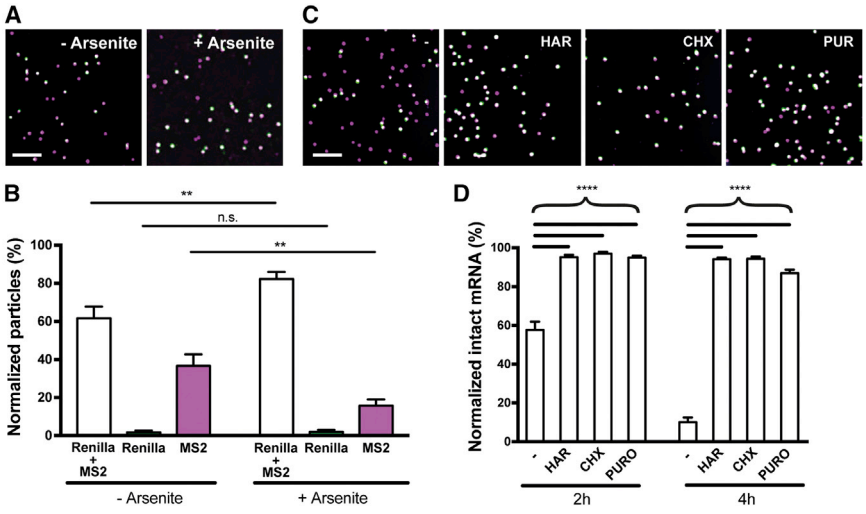

Figure 7. Stabilization of TREAT Transcripts during Stress and Translation Inhibition

(A) Representative smFISH images of the TREAT reporter in HeLa cells with and without arsenite stress. HeLa cells were induced for 2 hr with doxycycline and then treated with 500 μM arsenite for another 2 hr. Intact mRNAs (*Renilla* + MS2, white) and stabilized 3′ ends (MS2, magenta) were measured by smFISH.

(B) Intact mRNAs are stabilized in arsenite-stressed cells (16 cells) compared to unstressed cells (8 cells).

(C) Representative smFISH images of the TREAT reporter in HeLa cells treated with translational inhibitors. HeLa cells were induced for 2 hr with doxycycline followed by addition of translational inhibitors harringtonine (5 μM), cycloheximide (100 μg mL^{-1}), and puromycin (100 μg mL^{-1}) for 2 or 4 hr.

(D) Quantification of smFISH of HeLa cells treated with translational inhibitors shows stabilization of TREAT mRNAs. Shown are untreated (2 hr, 20 cells; 4 hr, 23 cells), harringtonine (2 hr, 34 cells; 4 hr, 37 cells), cycloheximide (2 hr, 38 cells; 4 hr, 38 cells), and puromycin (2 hr, 39 cells; 4 hr, 36 hr). Graph shows mean ± SEM. p values: ** < 0.01, **** < 0.0001; n.s., not significant; unpaired t test. Scale bars, 5 μm.

multi-color, multi-focal plane microscopy may enable single mRNAs to be observed continuously while freely moving in the cytosol (Abrahamsson et al., 2013).

STAR★METHODS

Detailed methods are provided in the online version of this paper and include the following:

- KEY RESOURCES TABLE
- CONTACT FOR REAGENT AND RESOURCE SHARING
- EXPERIMENTAL MODEL AND SUBJECT DETAILS
  - Cell lines and tissue culture
- METHOD DETAILS
  - Plasmid construction
  - HeLa stable cell line construction
  - Northern Blot
  - RT-qPCR
  - Renilla luciferase assay
  - siRNA transfection
  - Western Blotting
  - Single-molecule FISH
  - Detection of mRNA spots from smFISH and co-localization analysis
  - Correction of co-localization data for detection efficiency
  - Modeling of mRNA half-lives from smFISH measurements
  - Stochastic simulation of mRNA decay
  - Immunofluorescence
  - Live-cell imaging of TREAT mRNAs
- QUANTIFICATION AND STATISTICAL ANALYSIS
  - Single particle tracking of mRNAs in live cells and track co-localization
  - Live-cell slicing analysis
  - Quantification and co-localization of mRNAs in P-bodies in living cells
  - Statistical Analysis
- DATA AND SOFTWARE AVAILABILITY

SUPPLEMENTAL INFORMATION

Supplemental Information includes eight figures, seven movies, one file of detailed protocols, and the track-based co-localization workflow used to identify intact and stabilized 3′ end TREAT reporter mRNAs and can be found with this article online at https://doi.org/10.1016/j.molcel.2017.09.030.

AUTHOR CONTRIBUTIONS

I.H. and F.V. performed experiments and analyzed data with help from A.V.K. and C.G.A.-R. (northern blot and smFISH) and J.E. (image analysis). Y.Z. and L.G. performed the mathematical modeling, and M.B.S. contributed to data normalization. J.A.C. wrote the manuscript with input from all of the authors.

ACKNOWLEDGMENTS

This work was supported by the Novartis Research Foundation (J.A.C., L.G.), the Swiss National Science Foundation grant 31003A_156477 (J.A.C), the SNF-NCCR RNA & Disease (J.A.C.), and the SystemsX.ch/MetastasiX project (M.B.S.). The authors thank J. Kieft (UC Denver) for advice on viral pseudoknots, K. Schönig (CIMH) for the parental HeLa 11ht cell line, L. Lavis (Janelia Farm) for providing Halo and SNAP dyes, T. Lionnet (Janelia Farm) for providing access to AIRLOCALIZE detection software, and J. Lykke-Andersen (UCSD) for sharing plasmids containing TNF-α AU-rich element and RPL32 5′-TOP sequences. We acknowledge L. Gelman and S. Bourke (FMI) for microscopy support and H. Kohler (FMI) for cell sorting. The authors thank W. Filipowicz, H. Grosshans, T. Lionnet, R. Singer, and D. Schübeler for their helpful suggestions.

Received: August 22, 2017
Revised: September 8, 2017
Accepted: September 21, 2017
Published: October 19, 2017

REFERENCES

Abrahamsson, S., Chen, J., Hajj, B., Stallinga, S., Katsov, A.Y., Wisniewski, J., Mizuguchi, G., Soule, P., Mueller, F., Dugast Darzacq, C., et al. (2013). Fast multicolor 3D imaging using aberration-corrected multifocus microscopy. Nat. Methods *10*, 60–63.

Anderson, P., Kedersha, N., and Ivanov, P. (2015). Stress granules, P-bodies and cancer. Biochim. Biophys. Acta *1849*, 861–870.

Banani, S.F., Lee, H.O., Hyman, A.A., and Rosen, M.K. (2017). Biomolecular condensates: organizers of cellular biochemistry. Nat. Rev. Mol. Cell Biol. *18*, 285–298.

Beard, C., Hochedlinger, K., Plath, K., Wutz, A., and Jaenisch, R. (2006). Efficient method to generate single-copy transgenic mice by site-specific integration in embryonic stem cells. Genesis *44*, 23–28.

Berg, H.C. (1993). Random Walks in Biology (Princeton University Press).

Berthold, M.R., Cebron, N., Dill, F., Gabriel, T.R., Kötter, T., Meinl, T., Ohl, P., Thiel, K., and Wiswede, B. (2009). KNIME - The Konstanz Information Miner: Version 2.0 and Beyond. ACM SIGKDD Explorations Newsletter *11*, 26–31.

Bhattacharyya, S.N., Habermacher, R., Martine, U., Closs, E.I., and Filipowicz, W. (2006). Relief of microRNA-mediated translational repression in human cells subjected to stress. Cell *125*, 1111–1124.

Boehm, V., Gerbracht, J.V., Marx, M.C., and Gehring, N.H. (2016). Interrogating the degradation pathways of unstable mRNAs with XRN1-resistant sequences. Nat. Commun. *7*, 13691.

Brengues, M., Teixeira, D., and Parker, R. (2005). Movement of eukaryotic mRNAs between polysomes and cytoplasmic processing bodies. Science *310*, 486–489.

Chang, C.T., Bercovich, N., Loh, B., Jonas, S., and Izaurralde, E. (2014). The activation of the decapping enzyme DCP2 by DCP1 occurs on the EDC4 scaffold and involves a conserved loop in DCP1. Nucleic Acids Res. *42*, 5217–5233.

Chapman, E.G., Costantino, D.A., Rabe, J.L., Moon, S.L., Wilusz, J., Nix, J.C., and Kieft, J.S. (2014a). The structural basis of pathogenic subgenomic flavivirus RNA (sfRNA) production. Science *344*, 307–310.

Chapman, E.G., Moon, S.L., Wilusz, J., and Kieft, J.S. (2014b). RNA structures that resist degradation by Xrn1 produce a pathogenic Dengue virus RNA. eLife *3*, e01892.

Chen, J., Nikolaitchik, O., Singh, J., Wright, A., Bencsics, C.E., Coffin, J.M., Ni, N., Lockett, S., Pathak, V.K., and Hu, W.S. (2009). High efficiency of HIV-1 genomic RNA packaging and heterozygote formation revealed by single virion analysis. Proc. Natl. Acad. Sci. USA *106*, 13535–13540.

Chu, C.Y., and Rana, T.M. (2006). Translation repression in human cells by microRNA-induced gene silencing requires RCK/p54. PLoS Biol. *4*, e210.

Cougot, N., Babajko, S., and Séraphin, B. (2004). Cytoplasmic foci are sites of mRNA decay in human cells. J. Cell Biol. *165*, 31–40.

Daigle, N., and Ellenberg, J. (2007). LambdaN-GFP: an RNA reporter system for live-cell imaging. Nat. Methods *4*, 633–636.

Damgaard, C.K., and Lykke-Andersen, J. (2011). Translational coregulation of 5'TOP mRNAs by TIA-1 and TIAR. Genes Dev. *25*, 2057–2068.

Decker, C.J., and Parker, R. (2012). P-bodies and stress granules: possible roles in the control of translation and mRNA degradation. Cold Spring Harb. Perspect. Biol. *4*, a012286.

Dunckley, T., and Parker, R. (1999). The DCP2 protein is required for mRNA decapping in Saccharomyces cerevisiae and contains a functional MutT motif. EMBO J. *18*, 5411–5422.

Elkon, R., Zlotorynski, E., Zeller, K.I., and Agami, R. (2010). Major role for mRNA stability in shaping the kinetics of gene induction. BMC Genomics *11*, 259.

Eulalio, A., Behm-Ansmant, I., Schweizer, D., and Izaurralde, E. (2007). P-body formation is a consequence, not the cause, of RNA-mediated gene silencing. Mol. Cell. Biol. *27*, 3970–3981.

Franks, T.M., and Lykke-Andersen, J. (2007). TTP and BRF proteins nucleate processing body formation to silence mRNAs with AU-rich elements. Genes Dev. *21*, 719–735.

Friedel, C.C., Dölken, L., Ruzsics, Z., Koszinowski, U.H., and Zimmer, R. (2009). Conserved principles of mammalian transcriptional regulation revealed by RNA half-life. Nucleic Acids Res. *37*, e115.

Funakoshi, Y., Doi, Y., Hosoda, N., Uchida, N., Osawa, M., Shimada, I., Tsujimoto, M., Suzuki, T., Katada, T., and Hoshino, S. (2007). Mechanism of mRNA deadenylation: evidence for a molecular interplay between translation termination factor eRF3 and mRNA deadenylases. Genes Dev. *21*, 3135–3148.

Gagnon, K.T., Li, L., Chu, Y., Janowski, B.A., and Corey, D.R. (2014). RNAi factors are present and active in human cell nuclei. Cell Rep. *6*, 211–221.

Garcia, J.F., and Parker, R. (2015). MS2 coat proteins bound to yeast mRNAs block 5′ to 3′ degradation and trap mRNA decay products: implications for the localization of mRNAs by MS2-MCP system. RNA *21*, 1393–1395.

Garneau, N.L., Wilusz, J., and Wilusz, C.J. (2007). The highways and byways of mRNA decay. Nat. Rev. Mol. Cell Biol. *8*, 113–126.

Gillespie, D.T. (1977). Exact Stochastic Simulation of Coupled Chemical Reactions. J. Phys. Chem. *81*, 2340–2361.

Gowrishankar, G., Winzen, R., Dittrich-Breiholz, O., Redich, N., Kracht, M., and Holtmann, H. (2006). Inhibition of mRNA deadenylation and degradation by different types of cell stress. Biol. Chem. *387*, 323–327.

Grimm, J.B., English, B.P., Chen, J., Slaughter, J.P., Zhang, Z., Revyakin, A., Patel, R., Macklin, J.J., Normanno, D., Singer, R.H., et al. (2015). A general method to improve fluorophores for live-cell and single-molecule microscopy. Nat. Methods *12*, 244–250, 3, 250.

Halstead, J.M., Lionnet, T., Wilbertz, J.H., Wippich, F., Ephrussi, A., Singer, R.H., and Chao, J.A. (2015). Translation. An RNA biosensor for imaging the first round of translation from single cells to living animals. Science *347*, 1367–1671.

Hao, S., and Baltimore, D. (2009). The stability of mRNA influences the temporal order of the induction of genes encoding inflammatory molecules. Nat. Immunol. *10*, 281–288.

Heinrich, S., Sidler, C.L., Azzalin, C.M., and Weis, K. (2017). Stem-loop RNA labeling can affect nuclear and cytoplasmic mRNA processing. RNA *23*, 134–141.

Hilgers, V., Teixeira, D., and Parker, R. (2006). Translation-independent inhibition of mRNA deadenylation during stress in Saccharomyces cerevisiae. RNA *12*, 1835–1845.

Hocine, S., Raymond, P., Zenklusen, D., Chao, J.A., and Singer, R.H. (2013). Single-molecule analysis of gene expression using two-color RNA labeling in live yeast. Nat. Methods *10*, 119–121.

Isken, O., and Maquat, L.E. (2007). Quality control of eukaryotic mRNA: safeguarding cells from abnormal mRNA function. Genes Dev. *21*, 1833–1856.

Jain, S., and Parker, R. (2013). The discovery and analysis of P Bodies. Adv. Exp. Med. Biol. *768*, 23–43.

Kedersha, N., and Anderson, P. (2007). Mammalian stress granules and processing bodies. Methods Enzymol. *431*, 61–81.

Kieft, J.S., Rabe, J.L., and Chapman, E.G. (2015). New hypotheses derived from the structure of a flaviviral Xrn1-resistant RNA: Conservation, folding, and host adaptation. RNA Biol. *12*, 1169–1177.

Kramer, S. (2017). Simultaneous detection of mRNA transcription and decay intermediates by dual colour single mRNA FISH on subcellular resolution. Nucleic Acids Res. *45*, e49.

Leung, A.K., Calabrese, J.M., and Sharp, P.A. (2006). Quantitative analysis of Argonaute protein reveals microRNA-dependent localization to stress granules. Proc. Natl. Acad. Sci. USA *103*, 18125–18130.

Lionnet, T., Czaplinski, K., Darzacq, X., Shav-Tal, Y., Wells, A.L., Chao, J.A., Park, H.Y., de Turris, V., Lopez-Jones, M., and Singer, R.H. (2011). A transgenic mouse for in vivo detection of endogenous labeled mRNA. Nat. Methods *8*, 165–170.

Lykke-Andersen, J. (2002). Identification of a human decapping complex associated with hUpf proteins in nonsense-mediated decay. Mol. Cell. Biol. *22*, 8114–8121.

Miller, C., Schwalb, B., Maier, K., Schulz, D., Dümcke, S., Zacher, B., Mayer, A., Sydow, J., Marcinowski, L., Dölken, L., et al. (2011). Dynamic transcriptome analysis measures rates of mRNA synthesis and decay in yeast. Mol. Syst. Biol. *7*, 458.

Moon, S.L., Anderson, J.R., Kumagai, Y., Wilusz, C.J., Akira, S., Khromykh, A.A., and Wilusz, J. (2012). A noncoding RNA produced by arthropod-borne flaviviruses inhibits the cellular exoribonuclease XRN1 and alters host mRNA stability. RNA *18*, 2029–2040.

Morisaki, T., Lyon, K., DeLuca, K.F., DeLuca, J.G., English, B.P., Zhang, Z., Lavis, L.D., Grimm, J.B., Viswanathan, S., Looger, L.L., et al. (2016). Real-time quantification of single RNA translation dynamics in living cells. Science *352*, 1425–1429.

Otsu, N. (1979). A Threshold Selection Method from Grey-Level Histograms. IEEE Trans. Syst. Man Cybern. *9*, 62–66.

Pichon, X., Bastide, A., Safieddine, A., Chouaib, R., Samacoits, A., Basyuk, E., Peter, M., Mueller, F., and Bertrand, E. (2016). Visualization of single endogenous polysomes reveals the dynamics of translation in live human cells. J. Cell Biol. *214*, 769–781.

Rabani, M., Levin, J.Z., Fan, L., Adiconis, X., Raychowdhury, R., Garber, M., Gnirke, A., Nusbaum, C., Hacohen, N., Friedman, N., et al. (2011). Metabolic labeling of RNA uncovers principles of RNA production and degradation dynamics in mammalian cells. Nat. Biotechnol. *29*, 436–442.

Raj, A., and van Oudenaarden, A. (2008). Nature, nurture, or chance: stochastic gene expression and its consequences. Cell *135*, 216–226.

Schindelin, J., Arganda-Carreras, I., Frise, E., Kaynig, V., Longair, M., Pietzsch, T., Preibisch, S., Rueden, C., Saalfeld, S., Schmid, B., et al. (2012). Fiji: an open-source platform for biological-image analysis. Nat. Methods *9*, 676–682.

Schoenberg, D.R., and Maquat, L.E. (2012). Regulation of cytoplasmic mRNA decay. Nat. Rev. Genet. *13*, 246–259.

Sheth, U., and Parker, R. (2003). Decapping and decay of messenger RNA occur in cytoplasmic processing bodies. Science *300*, 805–808.

Stoecklin, G., Mayo, T., and Anderson, P. (2006). ARE-mRNA degradation requires the 5′-3′ decay pathway. EMBO Rep. *7*, 72–77.

Tinevez, J.Y., Perry, N., Schindelin, J., Hoopes, G.M., Reynolds, G.D., Laplantine, E., Bednarek, S.Y., Shorte, S.L., and Eliceiri, K.W. (2017). TrackMate: An open and extensible platform for single-particle tracking. Methods *115*, 80–90.

Trcek, T., Larson, D.R., Moldón, A., Query, C.C., and Singer, R.H. (2011). Single-molecule mRNA decay measurements reveal promoter- regulated mRNA stability in yeast. Cell *147*, 1484–1497.

Trcek, T., Sato, H., Singer, R.H., and Maquat, L.E. (2013). Temporal and spatial characterization of nonsense-mediated mRNA decay. Genes Dev. *27*, 541–551.

van Dijk, E., Cougot, N., Meyer, S., Babajko, S., Wahle, E., and Séraphin, B. (2002). Human Dcp2: a catalytically active mRNA decapping enzyme located in specific cytoplasmic structures. EMBO J. *21*, 6915–6924.

Voigt, F., Eglinger, J., and Chao, J.A. (in press). Detection of the first round of translation: the TRICK assay. In RNA Detection, I. Gaspar, ed. (Springer).

Wang, C., Han, B., Zhou, R., and Zhuang, X. (2016). Real-Time Imaging of Translation on Single mRNA Transcripts in Live Cells. Cell *165*, 990–1001.

Weidenfeld, I., Gossen, M., Löw, R., Kentner, D., Berger, S., Görlich, D., Bartsch, D., Bujard, H., and Schönig, K. (2009). Inducible expression of coding and inhibitory RNAs from retargetable genomic loci. Nucleic Acids Res. *37*, e50.

Wu, B., Miskolci, V., Sato, H., Tutucci, E., Kenworthy, C.A., Donnelly, S.K., Yoon, Y.J., Cox, D., Singer, R.H., and Hodgson, L. (2015). Synonymous modification results in high-fidelity gene expression of repetitive protein and nucleotide sequences. Genes Dev. *29*, 876–886.

Wu, B., Eliscovich, C., Yoon, Y.J., and Singer, R.H. (2016). Translation dynamics of single mRNAs in live cells and neurons. Science *352*, 1430–1435.

Yamagishi, R., Hosoda, N., and Hoshino, S. (2014). Arsenite inhibits mRNA deadenylation through proteolytic degradation of Tob and Pan3. Biochem. Biophys. Res. Commun. *455*, 323–331.

Yamashita, A., Chang, T.C., Yamashita, Y., Zhu, W., Zhong, Z., Chen, C.Y., and Shyu, A.B. (2005). Concerted action of poly(A) nucleases and decapping enzyme in mammalian mRNA turnover. Nat. Struct. Mol. Biol. *12*, 1054–1063.

Yan, X., Hoek, T.A., Vale, R.D., and Tanenbaum, M.E. (2016). Dynamics of Translation of Single mRNA Molecules In Vivo. Cell *165*, 976–989.

Yen, J.C., Chang, F.J., and Chang, S. (1995). A new criterion for automatic multilevel thresholding. IEEE transactions on image processing: a publication of the IEEE Signal Processing Society *4*, 370–378.

Zeng, Y., and Cullen, B.R. (2002). RNA interference in human cells is restricted to the cytoplasm. RNA *8*, 855–860.

STAR★METHODS

KEY RESOURCES TABLE

REAGENT or RESOURCE	SOURCE	IDENTIFIER
Antibodies		
Mouse anti-Rrp40	Abcam	ab67661; RRID: AB_1140293
Rabbit anti-α-Tubulin	Abcam	ab18251; RRID: AB_2210057
Rabbit anti-Xrn1	Abcam	ab70259; RRID: AB_1271494
Mouse anti-Actin-pan	ThermoFisher Scientific	MA5-11869; RRID: AB_11004139
Anti-rabbit IRDye 800 CW	LI-COR	926-68071; RRID: AB_10956166
Anti-mouse IRDye 680 RD	LI-COR	926-32210; RRID: AB_621842
Goat anti-rabbit secondary antibody coupled to Alexa Fluor 647	Molecular Probes, Thermo Fisher Scientific	A27040; RRID: AB_2536101
Chemicals, Peptides, and Recombinant Proteins		
JF549 HaloTag Ligand	Grimm et al., 2015	N/A
JF549 SNAP-tag Ligand	Grimm et al., 2015	N/A
FluoroBrite DMEM	Life Technologies	A1896702
Lipofectamine 2000	ThermoFisher Scientific	11668027
Lipofectamine RNAiMAX	ThermoFisher Scientific	13778030
Doxycycline	Sigma	D9891-1G
Hygromycin	ThermoFisher Scientific	10687010
Ganciclovir	BioCat GmbH (TargetMol)	T0688-6-TM
Sodium Arsenite solution	Sigma	35000-1L-R
Harringtonine	LKT Laboratories	H0169-5mg
Cycloheximide	Sigma	C4859-1ML
Puromycin 10 mg/ml	Invivogen	ant-pr-1
TRIzol	Ambion/Life Technologies	15596-026
20% Paraformaldehyde (aqueous, 10×10 mL)	Electron Microscopy Sciences	15713
Amersham Hybond-N+ membrane	GE Healthcare	45-000-763
UltraPure 20x SSC Buffer	Life Technologies	15557036
Methylene Blue Hydrate	Sigma	28514-100G
FastStart Universal SYBR Green Master mix	Roche	4913850001
Actinomycin D	Sigma	A1410-2MG
Bovine Serum Albumin	Sigma	A2153-50G
Dextran sulfate	Sigma	D6001-50G
Formamide (deionized)	Ambion, Life Technologies	AM9342
ProLong Gold Antifade Mountant	Molecular Probes, Life Technologies	P36934
Critical Commercial Assays		
Bradford Protein Assay	BioRad	5000006
DIG-Starter Northern Blot Kit	Roche	000000012039672910
TURBO DNA-free Kit	Ambion, Thermo Fisher Scientific	AM1907
SuperScript Reverse Transcriptase III	Thermo Fisher Scientific	18080093
Renilla Luciferase Assay System	Promega	E2810
Deposited Data		
Unprocessed Image Data	This paper	https://doi.org/10.17632/52wjrtnz2r.1

(*Continued on next page*)

Continued

REAGENT or RESOURCE	SOURCE	IDENTIFIER
Experimental Models: Cell Lines		
HeLa 11ht	Weidenfeld et al., 2009	N/A
HeLa-11ht-TREAT + NLS-stdMCP-Halo + NLS-stdPCP-stdGFP (+ SNAP-Dcp1a)	This paper	N/A
HeLa-11ht-TREAT-siRNA + NLS-stdMCP-Halo + NLS-stdPCP-stdGFP (+ SNAP-Dcp1a)	This paper	N/A
HeLa-11ht-TREAT-ARE + NLS-stdMCP-Halo + NLS-stdPCP-stdGFP (+ SNAP-Dcp1a)	This paper	N/A
Oligonucleotides		
MISSION pLKO.1-puro firefly luciferase shRNA Control: CCGG **CGCTGAGTACTTCGAAATGTC**CTCGAG**GACATTTCGAAGT ACTCAGCG**TTTTT	Sigma Aldrich	SHC007
Renilla FISH probes: TCGTACACCTTGGAAGCCAT AGTGATCATGCGTTTGCGTT GTTCATTTGCTTGCAGCGAG AGTTGATGAAGGAGTCCAGC GCGTGCTTCTCGGAATCATA CAGCGTTACCATGCAGAAAA TCGATGTGAGGCACGACGTG GATGATGCATCTAGCCACGG TTACCCATTCCGATCAGATC GATCCAGGAGGCGATATGAG CAAGCGGTGAGGTACTTGTA TTTGGAAGGTTCAGCAGCTC GTGGCCCACAAAGATGATTT GAGTAGTGAAAGGCCAGACA TTGATCTTGTCTTGGTGCTC CACTCTCAGCATGGACGATG CAGGACTCGATCACGTCCAC ATATCCTCCTCGATGTCAGG CTCTTCGCTCTTGATCAGGG ATTCTCAAGCACCATTTTCT GCATGGTCTCGACGAAGAAG TTTCCGCATGATCTTGCTTG CTTGAATGGCTCCAGGTAGG GAGAGGGTAGGCCGTCTAAC TTAACGAGAGGGATCTCGCG GACAATCTGGACGACGTCGG GAAGGTAGGCGTTGTAGTTG GAACATCTTAGGCAGATCGT TGGAAAAGAACCCAGGGTCG CTTAGCTCCCTCGACAATAG TTCACGAACTCGGTGTTAGG CTTACCCATTTCATCTGGAG GCTCCACGAAGCTCTTGATG TACTGCTCGTTCTTCAGCAC	Biosearch Technologies	N/A

(*Continued on next page*)

Continued

REAGENT or RESOURCE	SOURCE	IDENTIFIER
MS2v4 FISH probes: TGCCGTTTGTAGGTAGGATC CGCTTGAAGATTGGACAGTG GACTGTAATGACAGTGGAGC CTGATGCTGCTGGAGTTTGA ATGTCCTGATGTAGTCGGAG ATCGTCGAGCGTTGAATGAT ATAGTGTCTGAGGCATGCTG GTGATCGTGCAGCCGTTTGA CGATAACGTAGAGGCAGTAG CTGATGCTCGTCGCAGAAGA ATCTGGTATGTCCGATGTTG	Biosearch Technologies	N/A
3′-probe for Northern blot: CTTCAATCGATTTCGCGCGGGATCCAGACCACCTCCCC TGCGAGCTAAGCTGGACAGCCAATGACGGGTAAGAGA GTGACATTTTTCACTAACCTAAGACAGGAGGGCCGTCA GAGCTACTGCCTAATCCAAAGACGGGTAAAAGTGATAA AAATGTATCACTCCAACCTAAGACAGGCGCAGCTTCCG AGGGATTTGAGAT	This paper	N/A
Renilla forward qPCR primer: ATGGCTTCCAAGGTGTAC	This paper	N/A
Renilla reverse qPCR primer: TAGTTGATGAAGGAGTCCA	This paper	N/A
GAPDH forward qPCR primer: CGCTCTCTGCTCCTCCTGTT	This paper	N/A
GAPDH reverse qPCR primer: CCATGGTGTCTGAGCGATGT	This paper	N/A
c-Myc forward qPCR primer: CAGCTGCTTAGACGCTGGATT	This paper	N/A
c-Myc reverse qPCR primer: GTAGAAATACGGCTGCACCGA	This paper	N/A
ON-TARGETplus Human Exosc3 siRNA – SMARTpool: CCUGAAUGCUAGAGCGUGC GUAUUAUUAGAGUCCGAAA ACUCUCAGCAGAAGCGGUA GUGAACACAUGACGUCAGA	Dharmacon	L-031955-01-0005
ON-TARGETplus Non-targeting Pool: UGGUUUACAUGUCGACUAA UGGUUUACAUGUUGUGUGA UGGUUUACAUGUUUUCUGA UGGUUUACAUGUUUUCCUA	Dharmacon	D-001810-10-05
ON-TARGETplus Human Xrn1 siRNA – SMARTpool: CUUCAUAGUUGGUCGGUAU GAACAUAUUACAUGACGAA AAUAAGAAGGUGCGAGUAA AAUAAUUACCUCAGCGUUA	Dharmacon	L-013754-01-0005
Recombinant DNA		
pCAGGS-FLPe-IRESpuro plasmid	Beard et al., 2006	Addgene ID 20733
TNF-α AU-rich element: GATTATTTATTATTTATTTATTATTTATTTATTTAC	Franks and Lykke-Andersen, 2007	N/A
5′-TOP of RPL32: TCCTCTCTTCCTCGGCGCTGCCTACGGAGGTGGCAGCCATC-TCCTTCTCGGC	Damgaard and Lykke-Andersen, 2011	N/A
Software and Algorithms		
Graphpad Prism 7.0a	https://www.graphpad.com	N/A
Fiji including the TrackMate plugin	Schindelin et al., 2012; Tinevez et al., 2017	N/A
KNIME Analytics Platform version 3.2.1	Berthold et al., 2009	N/A
Data File S1 (Track-basedColocalizationAnalysis.knwf)	Voigt et al., in press	N/A

(*Continued on next page*)

Continued

REAGENT or RESOURCE	SOURCE	IDENTIFIER
Other		
Ibidi 35mm glass bottom dishes	ibidi	NOVS81158-IBI
Mini-PROTEAN 4-20% SDS gels	BioRad	4561096
Trans-Blot Turbo Mini PVDF Transfer Packs	BioRad	170-4156
Methods S1	This paper	N/A

CONTACT FOR REAGENT AND RESOURCE SHARING

All plasmids generated in this study are available from Addgene. For any other reagents or questions, please contact the corresponding author, Jeffrey A. Chao (jeffrey.chao@fmi.ch).

EXPERIMENTAL MODEL AND SUBJECT DETAILS

Cell lines and tissue culture

All cell lines are derivatives of a HeLa cell line (HeLa-11ht) constitutively expressing the reverse tetracycline controlled transactivator (rtTA2-M2) for inducible expression that also contains a single FLP recombinase-mediated cassette exchange (RCME) site (Weidenfeld et al., 2009). Cells were grown at 37°C and 5% CO_2 in DMEM containing 4.5 g L^{-1} glucose, 4 mM L-Glutamine, 100 U mL^{-1} Penicillin, 100 μg mL^{-1} Streptomycin and 10% FBS (Sigma Aldrich). To creat stable cell lines, RMCE was performed by replacement of the hygromycin-thymidine kinase (positive/negative) selection cassette with the individual TREAT reporter constructs.

METHOD DETAILS

Plasmid construction

To generate the TREAT reporter, the sequence of the tandem West Nile Virus Kunjin (WNV_{KUN}) pseudoknots (PKs) from the 3′ UTR of the genomic viral RNA was inserted between either 12 or 24 copies of PP7 stem loops and 24 copies of MS2 stem loops. This cassette was placed in the 3′ UTR of a *Renilla* luciferase transcript whose expression is driven by a doxycycline-inducible promoter. The TREAT reporter is composed of a doxycycline-inducible promoter – chimeric β-globin/IgG intron – *Renilla* luciferase coding sequence– stop codon –12x (24x) PP7 stem loops – 2x PKs – 24x MS2 stem loops – constitutive transport element – SV40 poly(A). In order to enable single genomic integration in HeLa cells, the TREAT construct was flanked by recognition sites for the FLP recombinase.

A control dual-color reporter was generated by removal of the PKs from the TREAT construct and was used to benchmark co-localization experiments in fixed and live cells and determine detection efficiencies. To generate a TREAT siRNA reporter that can be cleaved by Ago2, a 21nt long sequence from the firefly luciferase ORF was placed between the PP7 stem loops and the PKs of the TREAT construct. The firefly siRNA target sequence (CGCTGAGTACTTCGAA ATGTC) corresponds to the MISSION pLKO.1-puro firefly luciferase shRNA control (SHC007, Sigma Aldrich). Lentiviral transduction was used to stably integrate the cognate shRNA into HeLa cells. To enhance interaction of TREAT mRNAs with P-bodies, the AU-rich elements from TNF-α (Franks and Lykke-Andersen, 2007) were cloned in front of the PKs or the 5′-TOP sequence from RPL32 (Damgaard and Lykke-Andersen, 2011) was inserted into the 5′ UTR of the TREAT reporter.

HeLa stable cell line construction

A day before transfection, 3×10^5 HeLa cells were seeded into a 6-well plate. The targeting plasmid that contained a TREAT reporter (2 μg) and pCAGGS-FLPe-IRESpuro plasmid (2 μg) were transfected using Lipofectamine 2000 (Invitrogen) according to the manufacturer's protocol (Beard et al., 2006). Transfected cells were selected for two days with 5 μg mL^{-1} puromycin (Invivogen) followed by 10-14 days of negative selection with 50 μM ganciclovir (BioCat GmbH (TargetMol)) in order to obtain single resistant colonies that had undergone RCME. Individual colonies were then tested for expression of TREAT reporters using the *Renilla* Luciferase Assay System (Promega) according to the manufacturer's instructions. Total protein concentration in the lysates was measured using the Bradford Protein Assay (BioRad Laboratories) and used for normalization of luciferase activity.

Northern Blot

HeLa cells (1.5×10^6) with and without expression of the fluorescent coat proteins were seeded in a 10-cm plate. The following day, cells were transiently transfected with 20 μg of plasmid DNA that expressed either the TREAT reporter or a control reporter lacking the viral PKs by Lipofectamine 2000 (Invitrogen) according to the manufacturer's instructions. The next day, expression of the reporters was induced by addition of doxycycline (1 μg mL^{-1}) for 16 hr. Total RNA was extracted from these cells using TRIzol (Ambion). The

concentration of isolated RNAs was measured using a Nanodrop (Thermo Scientific) and 5 μg of total RNA for each condition was loaded on a 1.2% denaturing agarose gel containing 2% formaldehyde. The resolved RNA was transferred onto an Amersham Hybond-N+ membrane (GE Healthcare) by capillary transfer overnight in UltraPure 20 x SSC (Invitrogen) at room temperature. After the RNA was UV-cross-linked to the membrane, methylene blue staining (0.04% (w/v) Methylene Blue (Sigma) in 500 mM NaOAc pH 5.1) was used to assess loading and transfer of the RNA.

An anti-sense RNA probe was designed to detect the 3′ end of the transcript. The RNA probes were synthesized using the DIG-Starter Northern Blot Kit (Roche), and detection of transcripts was performed using the same kit according to the manufacturer's instructions. In brief, the concentration of *in vitro* transcribed DIG-labeled RNA probe was estimated based on an evaluation of labeling efficiency. The membrane was incubated with ~50 ng mL^{-1} RNA probes for 16 hr at 68°C. Upon detection with an anti-DIG antibody, the chemiluminiscent signal of the membrane was detected using an Azure c300 (Axonlab).

RT-qPCR

HeLa cells (6×10^5) stably expressing the TREAT reporter were seeded the day before in a 15-cm tissue culture plates. Induction of reporter transcription was done as described for the smFISH half-life experiment for time points 0, 2, 4 and 8 hr. Total RNA was isolated using TRIzol (Ambion). Total RNA (5 μg) was DNase-treated (TURBO DNA-free Kit, Ambion) and reverse transcribed (SuperScript Reverse Transcriptase III, Thermo Fisher Scientific) using oligo-dT primers to generate cDNA. The abundance of TREAT reporter transcripts was determined by real-time qPCR using FastStart Universal SYBR Green Master mix (Roche) and normalized to an endogenous reference gene GAPDH using the ΔΔCt method. The data were fit to one phase exponential decay using Prism 7.0a (https://www.graphpad.com) in order to calculate the half-life of the TREAT mRNA.

The same procedure was performed when actinomycin D (10 μg mL^{-1}) (Sigma) was added to inhibit transcription of endogenous mRNA. In this experiment, 1 μg of total RNA was used to measure the half-life of c-Myc mRNA.

Renilla luciferase assay

One day in advance, HeLa cells (2.5×10^4) stably expressing the TREAT reporters were seeded into a 24-well plate. Expression of the reporter was induced the next day for 2 hr by addition of doxycycline followed by lysis with 100 μL Passive Lysis Buffer from the *Renilla* Luciferase Assay System (Promega). The lysate (5 μL) was used to measure *Renilla* activity according to the manufacturer's protocol, and 30 μL of the lysate was used for total protein measurement using the Bio-Rad Protein Assay (Bio-Rad) to normalize the data.

siRNA transfection

HeLa cells (2×10^6) stably expressing the TREAT reporter were seeded onto 10-cm dish one day before siRNA transfection. Using Lipofectamine RNAiMAX (Invitrogen) either siXrn1 (ON-TARGETplus Human Xrn1 siRNA – SMARTpool, Dharmacon), siRrp40 (ON-TARGETplus Human Exosc3 siRNA – SMARTpool, Dharmacon), or siCtrl (ON-TARGETplus Non-targeting Pool, Dharmacon) were transfected at a final concentration of 50nM. The transfected cells were re-plated 8 hr later as follows: 0.5×10^6 cells onto a 6-cm dish for subsequent western blot quantification of the knock down efficiency; 2.5×10^4 cells onto a glass coverslip placed in a 12-well plate for smFISH analysis. Both western blot and FISH procedures were started 48 hr after siRNA transfection.

Western Blotting

Cells were washed with 1x PBS and lysed in 200 μL Passive Lysis Buffer (Promega). After a 15 min incubation on ice, cells were collected by scraping and centrifuged at 12,000 rpm for 20 min at 4°C. The supernatant was mixed with Laemmli buffer (Bio-Rad) and boiled for 5 min at 95°C. The protein samples were resolved by SDS-PAGE on a 4%–20% gel (Bio-Rad) followed by transfer to a PVDF membrane. The membrane was blocked with 5% BSA (Sigma) in PBST (1x PBS with 0.1% (v/v) Tween) for 1 hr at room temperature and subsequently probed with antibodies diluted in the same blocking buffer supplemented for 4 hr at room temperature: mouse derived anti-Rrp40 (Abcam, ab67661, 1:500) and rabbit derived anti-α-Tubulin (Abcam, ab18251, 1:1,000); rabbit derived anti-Xrn1 (Abcam, ab70259, 1:1,000) and mouse derived anti-Actin-pan (ThermoFisher Scientific, MA5-11869, 1:2,500). The membrane was washed four times in PBST for 5 min. Secondary antibodies were diluted in the blocking buffer supplemented with 0.01% (v/v) SDS and applied to the membrane for 1 hr at room temperature: anti-rabbit IRDye 800 CW (LI-COR, 1:15,000) and anti-mouse IRDye 680 RD (LI-COR, 1:15,000). After washing the membrane four times in PBST for 5 min, the membrane was imaged using an Odyssey infrared imaging system (LI-COR) and quantitative densitometry was performed using Fiji (Schindelin et al., 2012).

Single-molecule FISH

HeLa cells (2×10^4) were seeded on glass coverslips placed in a 12-well tissue culture plate two days before smFISH was performed. To induce transcription, the medium was replaced by complete DMEM containing doxycycline (1 μg mL^{-1}) for 1.5 hr. Cells were washed extensively with 1x PBS to remove doxycycline in order to stop transcription of TREAT reporter mRNAs. Fresh DMEM was then added to the cells and they were returned to the incubator for an additional 30 min to enable nascent transcription of TREAT reporters to finish. Afterward, cells were fixed at successive time points using 4% paraformaldehyde (Electron Microscopy Sciences) in 1x PBS for 10 min. Following fixation cells were washed twice with 1x PBS before storage in 70% ethanol at 4°C.

Single-molecule RNA detection was performed using Stellaris FISH probes (Biosearch Technologies). Briefly, cells on coverslips were prehybridized in wash buffer (2x SSC (Invitrogen), 10% (v/v) formamide (Ambion)) twice for 5 min. Two sets of FISH probes were designed to detect the *Renilla* ORF (Quasar670) or MS2 stem loops in the 3′ UTR (Quasar570). Cells were then hybridized with a solution that contained 150nM of each FISH probes, 2x SSC, 10% (v/v) formamide, 10% (w/v) dextran sulfate (Sigma) for 4 hr at 37°C. Cells were washed twice with wash buffer for 30 min before counterstaining DNA with DAPI solution (500 μg L^{-1} in 1 x PBS) and mounted on slides using ProLong Gold Antifade Mountant (Molecular Probes).

In order to investigate the effect of oxidative stress and of translational inhibitors on mRNA stability, prior to smFISH, cells were induced for 2 hr by doxycycline followed by either a 2 or 4 hr incubation with: 500 μM arsenite (Sigma), 5 μM harringtonine (LKT Laboratories), 100 μg mL^{-1} cycloheximide (Sigma), 100 μg mL^{-1} puromycin (Invivogen).

Images were acquired using a wide-field microscope (Zeiss) with a Plan-APOCHROMAT 100x 1.4 NA oil objective equipped with an AxioCam 506 mono camera and an X-Cite 120 EXFO metal halide light source. Cells were optically sectioned using a 240 nm z-step, spanning a 5 μm z-depth. Exposure times of 1600 ms were used to acquire images of each plane in the channel for Quasar670, 800 ms in the channel for Quasar570, and 10 ms in the DAPI channel.

Detection of mRNA spots from smFISH and co-localization analysis

Single mRNAs were detected in maximum projections of images using the spot detection algorithm AIRLOCALIZE (Lionnet et al., 2011) written in MATLAB (MathWorks) providing sub-pixel positions of the spots as described previously (Halstead et al., 2015). To detect the diffraction-limited fluorescent spots, thresholding was adjusted for each set of images depending on the signal-to-noise ratio. Either a custom MATLAB script or a KNIME Analytics Platform (Berthold et al., 2009) workflow (allowing segmentation for nuclear and cytoplasmic fraction based on DAPI staining using the Otsu thresholding method [Otsu, 1979]) were used to evaluate pairwise spot co-localization from both FISH channels. *Renilla* and MS2 spots that were within a maximum distance of 5 pixels (225 nm) were considered to be co-localized and were classified as intact mRNAs. Orphan MS2 spots were defined as stabilized 3′ ends.

Correction of co-localization data for detection efficiency

As a result of imperfect detection of single particle fluorescent labels, the observed fraction of co-localized particles underestimates the true fraction. For example, a missed magenta label from a double-labeled particle causes it to be wrongly classified as a single-labeled green particle. In order to correct for this type of error, we assumed that particles and color channels are independent and that there is a fixed rate of detection for each color label (detection efficiency, $e_{magenta}$ and e_{green}).

The detection efficiencies are estimated from a control experiment in which all particles are known to be double-labeled, using the following equations: $e_{magenta} = (n_{magenta}+n_{white})/N$ and $e_{green} = (n_{green}+n_{white})/N$, where $n_{magenta}$, n_{green}, and n_{white} are the normalized numbers of magenta, green, and double-labeled particles, and N is the total number of particles. In practice, N is estimated from $N = n_{magenta}+n_{green}+n_{white}$, which underestimates its true value by the number of particles for which both labels have been missed (n_{black}). For relatively large detection efficiencies as the ones obtained here ($e > 0.85$), $n_{black} > 0.0225$ and using $n_{black} = 0$ is an acceptable approximation.

In an experiment where we do not know the number of double-labeled particles, we can now express the observed numbers of particles (n_x, where x is $_{magenta,\ green}$ or $_{white}$) in terms of the true underlying number of particles (m_x) and the above detection efficiencies. For example, assuming that labels are never detected if they are truly absent, magenta particles can be observed from truly magenta particles (if the magenta label was detected) and from truly white particles (if the magenta label was detected and the green label was not detected): $n_{magenta} = m_{magenta}\cdot e_{magenta}+m_{white}\cdot e_{magenta}\cdot(1-e_{green})$. Double labeled particles can only be detected from truly double labeled ones if both labels were detected: $n_{white} = m_{white}\cdot e_{magenta}\cdot e_{green}$. Solving these equations for the true particle numbers yields:

$$m_{white} = n_{white}/\left(e_{magenta}\cdot e_{green}\right),$$

$$m_{magenta} = n_{magenta}/e_{magenta} - m_{white}\cdot\left(1 - e_{green}\right),$$

$$m_{green} = n_{green}/e_{green} - m_{white}\cdot\left(1 - e_{magenta}\right).$$

Finally, the fraction of co-localized particles is obtained from the estimated true numbers using $f_{white} = m_{white}/(m_{magenta}+m_{green}+m_{white})$.

Means and 95%-confidence intervals (CI) of means for detection efficiencies ($e_{magenta}$ and e_{green}) and normalized counts (n_x) were estimated using data from multiple experiments (cells) by $\bar{x} \mp t* \cdot s/\sqrt{n}$, where $\bar{x}$ is the arithmetic mean over the measurements x_i from individual cells, t^* is the critical value corresponding to the 97.5% quantile for a t distribution with n-1 degrees of freedom, s is the standard deviation estimated from the x_i, and n is the number of cells. These confidence intervals were then propagated to the derived entities calculated using the formulas described above using the R package *propagate* (version 1.0-4) calculated based on first-order Taylor expansion.

Modeling of mRNA half-lives from smFISH measurements

In the absence of transcription, we assumed that the turnover of intact mRNAs and stabilized 3′ ends is described by the following three rate equations, which account for the degradation of these RNA species in terms of three single-step Poisson processes:

$$\frac{d[\mathrm{Nuc}]}{dt} = -\alpha[\mathrm{Nuc}]$$

$$\frac{d[\mathrm{Cyt}]}{dt} = \alpha[\mathrm{Nuc}] - \beta[\mathrm{Cyt}]$$

$$\frac{d[\mathrm{Deg}]}{dt} = \beta[\mathrm{Cyt}] - \gamma[\mathrm{Deg}]$$

where *Nuc* is the number of nuclear mRNAs, *Cyt* is the number of cytoplasmic mRNAs, and *Deg* is the number of stabilized 3′ ends, respectively, and α, β and γ are their decay rates.

We fitted the solutions of this model to the population-averaged intact mRNA and stabilized 3′ end numbers, and obtained $\alpha = 0.94 \pm 0.07\ \mathrm{hr}^{-1}$, and $\beta = 0.43 \pm 0.06\ \mathrm{hr}^{-1}$. $\gamma = 0.16 \pm 0.02\ \mathrm{hr}^{-1}$. The goodness of fit with adjusted R^2 for the rates was $\alpha = 0.99$, $\beta = 0.97$, and $\gamma = 0.98$.

For the TREAT siRNA reporter, we added an additional rate to model the cytoplasmic degradation of the 5′ end generated by slicing:

$$\frac{d[5'\mathrm{Deg}]}{dt} = \beta[\mathrm{Cyt}] - \delta[5'\mathrm{Deg}]$$

We obtained rates of $\alpha = 0.99 \pm 0.25\ \mathrm{hr}^{-1}$, $\beta = 5.45 \pm 0.52\ \mathrm{hr}^{-1}$, $\gamma = 0.17 \pm 0.04\ \mathrm{hr}^{-1}$, and $\delta = 4.27 \pm 0.70\ \mathrm{hr}^{-1}$. The goodness of fit with adjusted R^2 for the rates were $\alpha = 0.94$, $\beta = 0.97$, $\gamma = 0.96$, and $\delta = 0.89$.

Stochastic simulation of mRNA decay

To evaluate to what extent the experimental cell-to-cell variability in mRNA numbers can be predicted by a simple model, we assumed that degradation of intact mRNA and stabilized 3′ end are single-step Poisson processes. To this end, we performed kinetic Monte Carlo simulations using the Gillespie algorithm to solve the master equation associated to the refined model described above, using the same export and decay rates (Gillespie, 1977). To simulate the time evolution of the probability distributions of intact mRNA and stabilized 3′ end after induction was stopped, we took the experimental distributions of all mRNA species after removal of doxycycline as the initial condition (t = 0).

We performed the simulations using the calculated rate constants α, β, γ, and δ that were extracted from fitting the rate equations (thick red lines in Figure S5, 6). We generated confidence intervals by running the simulation with $\alpha \pm \varepsilon_\alpha,\ \beta \pm \varepsilon_\beta,\ \gamma \pm \varepsilon_\gamma\ ,\ \delta \pm \varepsilon_\delta$ where ε are the fitting errors on each parameter returned by the NonLinearModelFit function in Mathematica (red shaded areas in Figure S5, 6).

Immunofluorescence

The HeLa cells (2×10^5) expressing SNAP-Dcp1a fusion were seeded onto glass coverslips placed in 12-well plate 2 days prior the immunostaining. After pre-staining the cells with SNAP dye Janelia Fluor 549 (JF549) (Grimm et al., 2015), the cells were treated with arsenite (500 μM) for 1.5 hr to stress cells and increase P-body levels. All the downstream steps were carried out at room temperature while coverslips were protected from light. Cells were washed with 1x PBS and fixed with 4% paraformaldehyde (Electron Microscopy Sciences) in 1x PBS for 10 min, washed once in 100mM glycine in 1x PBS and twice in 1x PBS, and subsequently permeabilized by methanol for 5 min. Following permeabilization, cells were washed twice with 1x PBS and then blocked for 1 hr in 0.5% BSA in 1x PBS. Cells were then incubated with Xrn1 antibody (Abcam, ab70259; 1:500) diluted in 0.5% BSA in 1x PBS for 1 hr. Cells were washed three times in 0.5% BSA in 1x PBS for 5 min. Cells were then incubated with goat anti-rabbit secondary antibody coupled to Alexa Fluor 647 (Molecular Probes; 1:5,000) diluted in 0.5% BSA in 1x PBS for 30 min. Cells were washed twice with 0.5% BSA in 1x PBS and once only with 1x PBS for 5 min each time. Nucleus was quickly counterstained by DAPI (500 ng mL^{-1} in 1x PBS), washed twice with 1 x PBS and coverslips were mounted onto glass slides with ProLong Gold Antifade Mountant (Molecular Probes).

Image acquisition was performed using a wide-field microscope (Zeiss) with a Plan-APOCHROMAT 63x 1.4 NA oil objective equipped with an AxioCam 506 mono camera and an X-Cite 120 EXFO metal halide light source. Cells were optically sectioned using a 240 nm z-step, spanning a 5 μm z-depth. Exposure times of 800 ms were used to acquire images of each plane in the channel for SNAP(JF549)-Dcp1a, 800 ms in the channel for Xrn1-Alexa647 and 10 ms in the DAPI channel. The co-localization analysis between P-body markers, SNAP-Dcp1a fusion and Xrn1, was done using the Fiji (Schindelin et al., 2012) plugin Coloc2 to calculate the Pearson's correlation coefficient.

Live-cell imaging of TREAT mRNAs

In order to label TREAT reporter mRNAs for live-cell imaging, chimeric fusions of the bacteriophage coat proteins (PCP and MCP) with spectrally distinct fluorescent proteins were used. Synonymous tandem PP7 coat protein (stdPCP) was fused to synonymous tandem green fluorescent protein (stdGFP) and synonymous tandem MS2 coat protein (stdMCP) was fused to Halo protein (Wu et al., 2015). Both fluorescent proteins contain N-terminal nuclear localization signals (NLS) to concentrate the unbound proteins in the nucleus. NLS-stdMCP-Halo was labeled with an organic Halo dye (JF549) (Grimm et al., 2015). Fusion proteins were expressed from a constitutive ubiquitin C promoter and stably integrated into the HeLa cell line by lentiviral transduction using standard protocols. Several rounds of fluorescence activated cell sorting (FACS) were used to derive a cell population expressing the fluorescent fusion proteins at levels appropriate for single-molecule RNA imaging.

In order to visualize P-bodies in live cells, a SNAP-Dcp1a fusion protein was introduced by lentiviruses for constitutive expression. SNAP dye (JF646) (Grimm et al., 2015) was used to label the SNAP-Dcp1a fusion protein. Triple positive cells, expressing NLS-stdPCP-stdGFP, NLS-stdMCP-Halo and SNAP-Dcp1a were isolated by FACS.

Cells were imaged on a spinning-disk confocal microscope based on an Olympus IX81 inverted microscope equipped with a Yokogawa CSU-X1 scanhead with Borealis modification (Andor) using a 100x 1.45 NA PlanApo TIRFM oil immersion objective (Olympus). Images were collected on two precisely aligned back-illuminated EMCCD cameras (EvolveDelta, Photometrics). Solid-state lasers (491 nm, 561 nm, 633 nm; Cobolt) were used as excitation sources. Cells were maintained at a constant temperature of 37°C and 5% CO_2 within an incubation box. Images were acquired using Visiview (Visitron) as single planes at frame rates of 20 Hz (50 ms exposure).

QUANTIFICATION AND STATISTICAL ANALYSIS

Single particle tracking of mRNAs in live cells and track co-localization

Single particle tracking (SPT) and analysis of mRNA molecules was performed on 5 frames of 50 ms exposure time for each of the two registered channels individually. SPT was performed using the Fiji plugin TrackMate (Tinevez et al., 2017) for the nucleus and cytoplasm separately as described before (Voigt et al., in press). For spot detection, we used "LoG detector" with an "Estimated blob diameter" of 0.38-40 μm and defined the "Threshold" based on individual images. We used the "Simple LAP tracker" particle-linking algorithm and applied linking distances that were optimized for particle density. The resulting list of coordinates served as input for a custom-made track co-localization pipeline running in KNIME (Berthold et al., 2009).

Here, we performed a nearest neighbor spot analysis that classifies two spots as co-localizing if their distance is below the user defined threshold of 0.3μm. Tracks co-localized if they contained at least 2 co-localizing spot pairs. Tracks shorter than 3 frames were excluded from the analysis. All other unpaired tracks containing only the MS2 signal were classified as stabilized 3′ ends.

Live-cell slicing analysis

TREAT siRNA and control data were collected as described above and including at least 100 frames of 50 ms exposure time per acquisition. SPT and co-localization analysis of the TREAT siRNA and control live-cell data was performed via automated tracking and track pairing analysis in KNIME.

Automated Tracking and Track Pairing

To this aim, we generated a workflow that enables KNIME to run the Fiji plugin TrackMate (Tinevez et al., 2017) in batch mode and via a custom-made ImageJ2 plugin (KNIME Image Processing → ImageJ2 → FMI → Track Spots). All tracking parameters are chosen as described above. The ROI is generated from an inverted segmentation of the nucleus that results after blurring of the raw image (Gaussian Blur, $\sigma = 5.5$) and global thresholding. Spot co-localization and classification is performed as described above. However, to improve track statistics over long time course experiments (> 100 frames) and avoid redundant counting of co-localizing tracks that cannot always be tracked without violation of gap criteria, we implemented a track pairing algorithm that pairs all tracks into the same pair ID if they spatially co-localize ($\geq$2 spot co-localizations) at some point throughout the experiment. This method stitches co-localizing tracks together that have been interrupted at different time points due to detection errors.

Identification of Slicing Events

For identification of slicing events, we selected for intact tracks that cease to co-localize without one of their labels vanishing. To this aim, we determined the length of both tracks after the last co-localization frame and selected candidate tracks that are detectable for at least three frames after their last co-localization. To more easily identify false-positive track co-localizations, we generated a measure for track inter-label mobility. Specifically, we quantified relative spot movement by assessing the distances between co-localizing spots of both channels (GFP and Halo+JF_{549}). We then calculated squared displacements and instantaneous diffusion coefficients (Berg, 1993) that measure the relative mobility of spots belonging to both labels for each co-localizing track. We applied the empirically determined threshold of 0.1 $\mu m^2\ s^{-1}$ to filter out high inter-label mobility tracks and then manually inspected and verified the candidate slicing events.

Nuclear Segmentation and Distance Analysis

In order to assess the subcellular localization of the slicing events, we determined their distance from the nucleus. To this aim, we segmented the nucleus via Gaussian Blur ($\sigma = 5.5$) and global thresholding (Huang method) and determined the average distance

(of all co-localizing frames per track) from the closest nuclear boundary via a distance map. As control, we used all co-localizing tracks (6,244 particles, 125 cells) of the non-sliced control population reporters.

Bleach Correction and 5′ end Decay Analysis

To generate a bleach curve and determine fluorophore decay rates, we acquired a test dataset under identical experimental conditions using the non-sliced control cell line. We manually tracked and co-localized particles as described above but only included tracks longer than 50 frames in the analysis. To determine the bleach rate of each fluorophore, we described bleaching as exponential decay according to

$$I_0 = \frac{I}{e^{-\lambda t}}$$

where I_0 is the intensity at the beginning of the experiment and λ is the fluorophore decay rate.

In order to experimentally determine λ, we took the natural logarithm of the intensities ($\ln(e^{-\lambda t}) = -\lambda t$), fit linear regressions and extracted λ as the slope of the linear fit:

$$I = \lambda t + I_0$$

To look for evidence of rapid loss of the 5′ end signal from a dual-labeled transcript, we only looked at tracks with more than five co-localizations. We normalized their bleach-corrected NLS-PCP-GFP intensity in each frame against the averaged intensity of the first five frames of each track. To search for putative 5′ end decay candidates, we identified tracks where the NLS-PCP-GFP signal was lost at least two frames before the NLS-MCP-Halo signal due to either differences in the bleach rate of GFP compared to Halo or degradation of the 5′ end after slicing but before the 5′ and 3′ ends separated. We then fit a linear regression to the last five frames of the NLS-PCP-GFP track and determined its slope (*m*). Slopes were determined for both non-sliced control and the TREAT siRNA transcripts to identify possible 5′ end decay events that would have large negative values.

Quantification and co-localization of mRNAs in P-bodies in living cells

Intact and degraded mRNAs were identified by measuring the co-localization of NLS-PCP-GFP and NLS-MCP-Halo tracks as described previously. P-bodies were identified based upon segmentation of the SNAP-Dcp1a fluorescent signal (using the Yen thresholding method (Yen et al., 1995) in KNIME (Berthold et al., 2009) workflow) and used to generate distance maps that measured the number of pixels inside and outside of P-bodies. By overlaying the mRNA tracks with the distance map, we defined pixel positions within P-bodies as positive and positions outside of P-bodies as negative. The position of intact and stabilized 3′ ends with respect to P-bodies was then measured at each frame and the cumulative P-body localization index was then calculated for RNA particles in three consecutive frames.

The RNA content per P-body was determined by quantification of the NLS-PCP-GFP and NLS-MCP-Halo fluorescence intensities per frame of all dual labeled particles using TrackMate (Tinevez et al., 2017) + KNIME (Berthold et al., 2009). The ratio of the two channels was then calculated for all co-localizing spots and compared with the intensity ratio determined for intact mRNAs in the cytosol.

Statistical Analysis

Statistical parameters are shown in the figures and listed in the figure legends. Statistical significance is claimed when $p < 0.05$ in a Student's t test. In figures, asterisks mark statistical significance as following *, $p < 0.05$; **, $p < 0.01$; ***, $p < 0.001$; ****, $p < 0.0001$.

DATA AND SOFTWARE AVAILABILITY

All KNIME workflows are available from the Chao lab upon request. The ImageJ2 plugin that enables TrackMate to run in KNIME has been uploaded into the KNIME Image Processing library. The track-based co-localization workflow Data S1 ("Track-basedColocalizationAnalysis.knwf") used to identify intact and stabilized 3′ end TREAT reporter mRNAs is available as a supplemental item to this manuscript.

The unprocessed image files used to prepare the figures in this manuscript have been deposited at Mendeley Data (https://doi.org/10.17632/52wjrtnz2r.1)